Title
Small-Molecule Patterning via Prefunctionalized Alkanethiols

Journal
Chemistry of Materials, 30(12)

ISSN
0897-4756

Authors
Cao, Huan H
Nakatsuka, Nako
Deshayes, Stephanie
et al.

Publication Date
2018-06-26

DOI
10.1021/acs.chemmater.8b00377

Peer reviewed

HHS Public Access

Author manuscript

Chem Mater. Author manuscript; available in PMC 2019 February 28.

Published in final edited form as:

Chem Mater. 2018 June 26; 30(12): 4017–4030. doi:10.1021/acs.chemmater.8b00377.

Small-Molecule Patterning via Prefunctionalized Alkanethiols

Huan H. Cao[#1,2], **Nako Nakatsuka**[#1,2], **Stephanie Deshayes**[3], **John M. Abendroth**[1,2], **Hongyan Yang**[4], **Paul S. Weiss**[1,2,5,*], **Andrea M. Kasko**[2,3,*], and **Anne M. Andrews**[1,2,4,*]

[1]Department of Chemistry and Biochemistry, University of California, Los Angeles, Los Angeles, CA 90095, United States

[2]California NanoSystems Institute, University of California, Los Angeles, Los Angeles, CA 90095, United States

[3]Department of Bioengineering, University of California, Los Angeles, Los Angeles, CA 90095, United States

[4]Department of Psychiatry and Biobehavioral Sciences, Semel Institute for Neuroscience and Human Behavior, and Hatos Center for Neuropharmacology, David Geffen School of Medicine, University of California, Los Angeles, Los Angeles, CA 90095, United States

[5]Department of Materials Science and Engineering, University of California, Los Angeles, Los Angeles, CA 90095, United States

[#] These authors contributed equally to this work.

Abstract

Interactions between small molecules and biomolecules are important physiologically and for biosensing, diagnostic, and therapeutic applications. To investigate these interactions, small molecules can be tethered to substrates through standard coupling chemistries. While convenient, these approaches co-opt one or more of the few small-molecule functional groups needed for biorecognition. Moreover, for multiplexing, individual probes require different surface functionalization chemistries, conditions, and/or protection/deprotection strategies. Thus, when placing multiple small-molecules on surfaces, orthogonal chemistries are needed that preserve all functional groups and are sequentially compatible. Here, we approach high-fidelity small-molecule patterning by coupling small-molecule neurotransmitter precursors, as examples, to monodisperse asymmetric oligo(ethylene glycol)alkanethiols during synthesis and *prior* to self-assembly on Au substrates. We use chemical lift-off lithography to singly and doubly pattern substrates. Selective antibody recognition of pre-functionalized thiols was comparable to or better than recognition of small molecules functionalized to alkanethiols *after* surface assembly. These

[*]**Corresponding Authors** aandrews@mednet.ucla.edu, akasko@ucla.edu, or psw@cnsi.ucla.edu.

AUTHOR CONTRIBUTIONS

Experiments were carried out by HHC, NN, SD, and JMA. Data analysis, figure preparation, and writing was by all authors, who approved the final version and agree to be accountable for the accuracy and integrity of the work.

Supporting Information

Insertion time dependence, antibody descriptions, X-ray photoelectron spectroscopy data, scan-rate dependence for electrochemistry, and representative fluorescence images for control experiments corresponding to main text figures are available free of charge *via* the Internet at http://pubs.acs.org.

NOTES

The authors declare no competing financial interest.

findings demonstrate that synthesis and patterning approaches that circumvent sequential surface conjugation chemistries enable biomolecule recognition and afford gateways to multiplexed small-molecule functionalized substrates.

Table of contents image

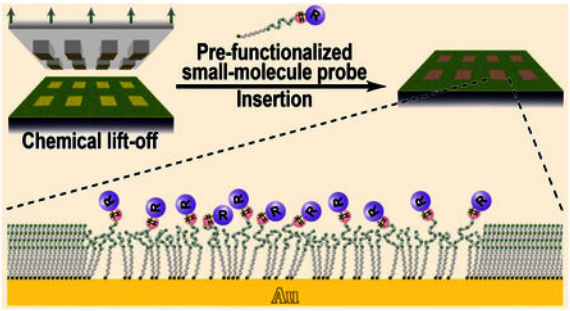

Keywords

lithography; chemical patterning; self-assembly; neurotransmitter; biorecognition; fluorescence microscopy

INTRODUCTION

We have investigated general design rules for small-molecule surface functionalization to improve recognition by biomolecules.[1–6] In parallel, we developed readily adoptable small-molecule patterning methods.[7–10] Patterning enables relative molecular recognition between functionalized (patterned) and unfunctionalized (control) regions to be compared and quantified on the same substrate. Molecular level patterning *via* inserting tethers into self-assembled monolayers[11–13] is advantageous for spacing small-molecule probes so that large biomolecule targets have ample access for recognition with minimal steric hindrance.[6,14] We demonstrated that linking chemistries for small molecules where an extra functional group is used for surface-tethering, is essential for native biomolecule recognition.[2,4] Controlling surface chemistries to reduce nonspecific substrate interactions is another critical factor that others and we have addressed.[1,4,15,16]

We previously used multiplexed substrates produced *via* chemical lift-off lithography and microfluidics to sort antibodies or membrane-associated receptors from mixtures to their cognate small-molecule partners.[2,17] However, the on-substrate conjugation chemistries employed, *e.g.*, NHS-EDC coupling, suffer from incomplete functionalization and possible by-product formation, which likely contribute to surface-to-surface variation and nonspecific recognition.[18–20] On-substrate sequential functionalization is difficult to control and to bring to completion with high yields.[21] The extent of reaction differs with specific probes.[2] Moreover, monodisperse surface-functionalization is challenging due to the formation of clusters or domains of molecules arising from phase separation in mixed monolayers.[22–24]

In light of these and other shortcomings, we decided to investigate small-molecule-functionalized substrates using a “pre-functionalized” synthesis approach. Small-molecule oligo(ethylene glycol)-terminated alkanethiols are not readily available. Moreover, synthesis requires heterobifunctionalization and orthogonal chemistries to couple different small-molecule tail groups. To address these challenges, we developed a synthetic route to a library of monodisperse hepta(ethylene glycol)undecyl pyridyl disulfides (7EG-PDS) pre-functionalized with neurotransmitter mimics, *i.e.*, *L*-3,4-dihydroxyphenylalanine (*L*-DOPA), *L*-threo-3,4-dihydroxyphenylserine (*L*-DOPS), *L*-5-hydroxytryptophan (*L*-5-HTP), *L*-histidine (*L*-HD), and *L*-tryptophan (*L*-Trp) (Figure 1A).

The small-molecule probes investigated are naturally occurring proximal precursors to monoamine neurotransmitters, *i.e.*, dopamine, norepinephrine, serotonin, and histamine, respectively. The exception is *L*-tryptophan from which serotonin is synthesized in two enzymatic steps by way of *L*-5-HTP *in vivo*. By using neurotransmitter amino acid precursors, as depicted in Figure 1A, we introduced an additional carboxyl moiety for tethering, thereby preserving amino groups for biorecognition.[4,25,26] Substrates functionalized with neurotransmitter precursors mimic biologically active (free) neurotransmitters in terms of selective molecular recognition of the corresponding native membrane-associated receptors.[2,4]

Herein, we refer to mimicking precursors as neurotransmitters (unless otherwise noted). We denote tethers functionalized with neurotransmitters prior to self-assembly as pre-functionalized thiols and tethers that are self-assembled and then functionalized with neurotransmitters as post-functionalized thiols. Substrates modified with pre-functionalized *vs.* post-functionalized thiols were patterned using chemical lift-off lithography[9,10] (Figure 1B,C). Since 7EG-PDS molecules were conjugated with small-molecule probes *prior* to surface assembly and patterning, the need to devise compatible multi-step functionalization chemistries and to optimize reaction conditions for coupling each neurotransmitter on-substrate was obviated. Using antibodies as test systems, we directly compared differences in biomolecule target recognition of pre-functionalized *vs.* post-functionalized small-molecule probes.

EXPERIMENTAL SECTION

Materials.

Silicon substrates with Au films (100-nm-thick overlaying 10-nm-thick Ti adhesive layers) were purchased from Platypus Technologies (Madison, WI, USA). (11-Mercaptoundecyl) tri(ethylene glycol) (TEG) was purchased from Toronto Research Chemicals Inc. (Toronto, ON, Canada). (11-Mercaptoundecyl) hexa(ethylene glycol)amine (AEG) was obtained from ProChimia Surfaces (Sopot, Poland). Threo-3,4-dihydroxyphenylserine (*L*-DOPS or *L*-droxidopa) was purchased from TCI America Inc. (Portland, OR, USA). Fluorenylmethyloxycarbonyl chloride (Fmoc-Cl) was from Oakwood Products (West Columbia, SC, USA). Sodium carbonate (Na_2CO_3) was purchased from Fisher Scientific. Dichloromethane (DCM) was obtained from Fisher Scientific and distilled over calcium hydride (CaH_2).

9-Fluorenylmethyloxycarbonyl-*L*-3,4-dihydroxyphenylalanine (Fmoc-*L*-DOPA-OH), 9-fluorenylmethyloxycarbonyl-5-hydroxy-*L*-tryptophan (Fmoc-*L*-5-HTP-OH), and *N*-α-(9-fluorenylmethyloxycarbonyl)-*N*-im-trityl-*L*-histidine (Fmoc-*L*-His(Trt)-OH) were from AnaSpec-Eurogentec (Fremont, CA, USA). The *N*-*α*-(9-fluorenylmethyloxycarbonyl)-*N*-in-*tert*-butyloxycarbonyl-*L*-tryptophan (Fmoc-*L*-Trp(Boc)-OH) and hexa(ethylene glycol) molecules were from ChemPep Inc. (Wellington, FL, USA). 11-Bromo-1-undecene, thioacetic acid (CH_3COSH), triethylamine (TEA), triphenylphosphine (Ph_3P), and *N,N*-diisopropylethylamine (DIEA) were purchased from Alfa Aesar (Ward Hill, MA, USA). The NHS, EDC, DMF, 4-methylpiperidine, BSA, 0.01 M PBS (138 mM NaCl, 2.7 mM KCl, 10 mM Na_2HPO_4, 1.8 mM KH_2PO_4, pH 7.4), and azobisisobutyronitrile (AIBN) were purchased from Sigma-Aldrich (St. Louis, MO, USA).

4-Toluenesulfonyl chloride (TsCl), 2,2'-dithiodipyridine (2-PDS), ammonia (7 N in MeOH), and trifluoroacetic acid (TFA) were from Acros Organics (Geel, Belgium). Anhydrous tetrahydrofurane (THF), anhydrous methanol (MeOH), and sodium azide (NaN_3) were obtained from EMD Chemicals (Gibbstown, NJ, USA). Hydroxybenzotriazole (HOBt) was purchased from CreoSalus Inc. (Louisville, KY, USA). *SYLGARD®* 184 silicone elastomer kits were from Ellsworth Adhesives (Germantown, WI, USA). Absolute (200 proof) ethanol (EtOH) was purchased from Decon Laboratories, Inc. (King of Prussia, PA, USA). Deionized water (~18 MΩ) was obtained from a Millipore water purifier (Billerica, MA, USA).

Mouse monoclonal anti-*L*-3,4-dihydroxyphenylalanine antibody (ascites), rabbit polyclonal anti-*L*-5-hydroxytryptophan antibody (whole antiserum), rabbit polyclonal anti-*L*-histidine antibody (whole antiserum), and rat polyclonal anti-*L*-tryptophan antibody (pre-adsorbed antiserum) were purchased from Abcam, Inc. (Cambridge, MA, USA). AlexaFluor® 546 goat anti-rabbit IgG (H+L) highly cross-adsorbed antibody (2 mg/mL), AlexaFluor® 568 goat anti-rat IgG (H+L) antibody (2 mg/mL), AlexaFluor® 488 goat anti-rabbit IgG (H+L) antibody (2 mg/mL), and AlexaFluor® 488 goat anti-mouse IgG (H+L) highly cross-adsorbed antibody (2 mg/mL) were purchased from Invitrogen (Carlsbad, CA, USA). All primary and secondary antibodies were diluted 1:200 and 1:100, respectively, with 0.01 M PBS pH 7.4 prior to incubation with substrates, unless stated otherwise.

Synthesis of Fmoc-*L*-DOPS-OH.

A solution of 208.5 mg (0.98 mmol, 1 eq.) of *L*-DOPS in 10 mL of a 2:1 mixture of 10% aqueous Na_2CO_3/THF was cooled to 0 °C in an ice bath and a solution of Fmoc-Cl (278.9 mg, 1.08 mmol, 1.1 eq.) in THF (3.4 mL) was added dropwise. The reaction was stirred overnight at room temperature. The THF was evaporated under reduced pressure and the compound was extracted with ethyl acetate. The aqueous layer was acidified to pH 2 with 6 M HCl and was then extracted again with ethyl acetate. The organic extract was dried over magnesium sulfate, filtered, and then rotovapped to dryness. The oil was purified by silica gel chromatography (eluent: DCM/ethyl acetate 9:1 to 1:9 and DCM/MeOH 19:1) to give 344 mg of a light brown solid (79%). ^{1}H NMR (300 MHz, DMSO-*d6*, 25 °C): *d* (ppm) = 8.80 (s, 1 H), 8.75 (s, 1 H), 7.88 (d, 2 H, J = 7.6 Hz), 7.61–7.71 (m, 2 H), 7.25–7.45 (m, 4 H), 7.07 (d, 1 H, J = 9.2 Hz), 6.78 (s, 1 H), 6.62–6.66 (m, 2 H), 4.94 (m, 1 H), 4.05–4.24 (m,

4 H), 3.17 (d, 1 H, J = 5.04 Hz). Mass analysis (MALDI-TOF): m/z 458.9754 (calculated for $C_{24}H_{21}NNaO_7$ $[M+Na]^+$ m/z 458.1210).

Synthesis of Undec-1-en-11-ylhepta(ethylene glycol) (1).

Undec-1-en-11-ylhepta(ethylene glycol) was synthesized as previously described.[27] Hepta(ethylene glycol) (4.95 g, 15.2 mmol, 3 eq.) was treated with 606 mg of 50% aqueous sodium hydroxide solution (7.6 mmol, 1.5 eq.) for 30 min at 100 °C under argon, and then 11-bromo-1-undecene (1.18 g, 5.05 mmol, 1 eq.) was added. The solution was stirred for 24 h at 100 °C under argon, then cooled down. The organic mixture was extracted with DCM and purified by silica gel chromatography (eluent: ethyl acetate to remove the di-functionalized molecule, then DCM/MeOH 19:1 to obtain the mono-functionalized molecule, and finally DCM/MeOH 9:1 to recover the non-modified hepta(ethylene glycol)) giving 1.51 g of the mono-functionalized compound **1** (colorless oil, 63%). ^{1}H NMR (300 MHz, deuterated chloroform ($CDCl_3$), 25 °C): *d* (ppm) = 5.74–5.89 (m, 1 H), 4.89–5.04 (m, 2 H), 3.53–3.77 (m, 28 H), 3.44 (t, 2 H, J = 6.8 Hz), 2.67 (br s, 1 H), 2.04 (q, 2 H, J = 7.1 Hz), 1.57 (quin, 2 H, J = 7.0 Hz), 1.22–1.43 (m, 12 H). Mass analysis (MALDI-TOF): m/z 501.2800 (calculated for $C_{25}H_{50}NaO_8$ $[M+Na]^+$ m/z 501.3398).

Synthesis of [1-[(Methylcarbonyl)thio]undec-11-yl]hepta(ethylene glycol) (2).

[1-[(Methylcarbonyl)thio]undec-11-yl]hepta(ethylene glycol) was synthesized as previously described with slight modifications.[27] Compound **1** (587.2 mg, 1.23 mmol, 1 eq.) was dissolved in 4 mL of anhydrous MeOH. Thioacetic acid (351 *m*L, 4.92 mmol, 4 eq.) and 10 mg of AIBN were added. The mixture was irradiated with a UV lamp (UVP XX-40 BLB, 40 W, 365 nm) for 24 h. Afterwards, another 10 mg of AIBN was added and the reaction was stirred for an additional 24 h before concentration by rotary evaporation followed by purification by silica gel chromatography (eluent: ethyl acetate, then DCM/MeOH 19:1). Then 618.7 mg of compound **2** (91%) were obtained as a colorless oil. ^{1}H NMR (300 MHz, $CDCl_3$, 25 °C): *d* (ppm) = 3.54–3.78 (m, 28 H), 3.44 (t, 2 H, J = 6.8 Hz), 2.86 (t, 2 H, J = 7.3 Hz), 2.77 (br s, 1 H), 2.32 (s, 3 H), 1.50–1.63 (m, 4 H), 1.21–1.41 (m, 14 H). Mass analysis (MALDI-TOF): m/z 577.6519 (calculated for $C_{27}H_{54}NaO_9S$ $[M+Na]^+$ m/z 577.3381).

Synthesis of [1-[(Methylcarbonyl)thio]undec-11-yl]-21-(tosyl)oxy-1,4,7,10,13,16, 19 heptaoxaheneicosane (3).

To a solution of compound **2** (1.29 g, 2.32 mmol, 1 eq.) in distilled DCM (2 mL), triethylamine (648 *m*L, 4.64 mmol, 2 eq.) was added. The solution was cooled to 0 °C in an ice bath and TsCl (663 mg, 3.48 mmol, 1.5 eq.) was added. The ice bath was then removed and the solution was allowed to warm to room temperature and react for 24 h. The resultant mixture was diluted in DCM (50 mL) and washed with 2% acetic acid solution and brine. The organic layer was dried with magnesium sulfate and then rotovapped to remove all remaining liquid. The compound was purified by silica gel chromatography (eluent: DCM/ethyl acetate 4:1–1:1). Then 1.26 g of compound **3** (76%) were obtained as a colorless oil. ^{1}H NMR (500 MHz, $CDCl_3$, 25 °C): *d* (ppm) = 7.80 (d, 2 H, J = 8.1 Hz), 7.34 (d, 2 H, J = 8.1 Hz), 4.16 (t, 2 H, J = 4.9 Hz), 3.69 (t, 2 H, 4.9 Hz), 3.56–3.67 (m, 24 H), 3.44 (t, 2 H, J = 6.9 Hz), 2.86 (t, 2 H, J = 7.1 Hz), 2.45 (s, 3 H), 2.32 (s, 3 H), 1.52–1.62 (m, 4 H), 1.22–1.41

(m, 14 H). Mass analysis (MALDI-TOF): m/z 731.3299 (calculated for $C_{34}H_{60}NaO_{11}S_2$ [M +Na]$^+$ m/z 731.3469).

Synthesis of [1-Mercaptoundec-11-yl]-21-azido-1,4,7,10,13,16,19-heptaoxaheneicosane(4).

To a solution of compound **3** (1.26 g, 1.77 mmol, 1 eq.) in absolute EtOH (21 mL), NaN_3 (230 mg, 3.54 mmol, 2 eq.) was added. The solution was stirred at 85 °C overnight under argon. Afterward, the solution was cooled to room temperature. The solvent was carefully evaporated under reduced pressure; then the salts were precipitated in ethyl acetate and removed by filtration. The solution was rotovapped to dryness yielding 902.5 mg (94%) of compound **4** (and its disulfide derivative) as colorless oil. The residue was used as is without further purification. The thioacetate group was cleaved inducing the formation of disulfide bonds (~50%). ^{1}H NMR (500 MHz, $CDCl_3$, 25 °C): *d* (ppm) = 3.49–3.83 (m, 26 H), 3.44 (t, 2 H, J = 6.7 Hz), 3.39 (t, 2 H, J = 4.7 Hz), 2.68 (t, 2 H, J = 7.3 Hz, CH_2-S-S), 2.52 (q, 2 H, J = 7.2 Hz, CH_2-SH), 1.66 (quin, 2 H, J = 7.3 Hz), 1.57 (quin, 2 H, J = 7.5 Hz), 1.20–1.40 (m, 14 H). Mass analysis (MALDI-TOF): m/z 560.3625 (calculated for $C_{25}H_{51}N_3NaO_7S$ [M +Na]$^+$ m/z 560.3345) and m/z 1095.7825 for the disulfide derivative (calculated for $C_{50}H_{100}N_6NaO_{14}S_2$ [M+Na]$^+$ m/z 1095.6637).

Synthesis of [1-(Pyridin-2-yldisulfanyl)undec-11-yl]-21-amino 1,4,7,10,13,16,19 heptaoxaheneicosane (amine hepta(ethylene glycol)-terminated undecane-pyridyl disulfide (7EG-PDS) (5).

A solution of compound **4** (902.5 mg, 1.68 mmol, 1 eq.) in anhydrous THF (5 mL) was cooled to 0 °C in an ice bath and triphenylphosphine (818 mg, 3.12 mmol, 1.9 eq.) was added under argon. The ice bath was then removed and the solution was allowed to warm to room temperature and react for 24 h. The solvent was evaporated under reduced pressure and water was added to the mixture. The solution was filtered to remove precipitated triphenylphosphine oxide. The filtrate was then rotovapped to dryness yielding 1.03 g of a crude compound. The residue was dissolved in 20 mL of ammonia solution (7 N in MeOH), and 2-PDS (1.95 g, 8.85 mmol, 5.3 eq.) was added to the mixture under argon. The solution was stirred for 72 h at room temperature. The solvent was removed by rotary evaporation. The resultant mixture was diluted in DCM (100 mL) and washed with water. The organic layer was dried with magnesium sulfate and then rotovapped to dryness. The compound was dissolved in water, washed with hexane (4 times) and lyophilized. Then 474 mg of compound **5** (45%) were obtained as a colorless oil. ^{1}H NMR (500 MHz, $CDCl_3$, 25 °C): *d* (ppm) = 8.46 (d, 1 H, J = 4.7 Hz), 7.73 (d, 1 H, J = 8.2 Hz), 7.64 (t, 1 H, J = 7.0 Hz), 7.08 (t, 1 H, J = 6.2 Hz), 3.54–3.76 (m, 26 H), 3.44 (t, 2 H, J = 6.8 Hz), 2.99 (t, 2 H, J = 4.1 Hz), 2.79 (t, 2 H, J = 7.2 Hz), 1.68 (quin, 2 H, J = 7.2 Hz), 1.56 (quin, 2 H, J = 6.4 Hz), 1.19–1.45 (m, 14 H). Mass analysis (MALDI-TOF): m/z 621.3679 (calculated for $C_{30}H_{57}N_2O_7S_2$ [M +H]$^+$ m/z 621.3602).

Synthesis of Fmoc-*L*-DOPA-7EG-PDS (6a).

Fmoc-*L*-DOPA-OH (88 mg, 0.21 mmol, 1.1 eq.) was coupled to 7EG-PDS compound **(5)** (120 mg, 0.19 mmol, 1 eq.) according to the general procedure described above. Then, 81 mg of compound **6a** (42%) were obtained as a colorless oil. ^{1}H NMR (300 MHz, $CDCl_3$,

25 °C): *d* (ppm) = 8.45 (m, 1 H), 7.25–7.76 (m, 10 H), 7.05–7.10 (m, 1 H), 6.56–6.84 (m, 3 H), 6.03 (m, 1 H), 5.70 (m, 1 H), 4.18–4.44 (m, 4 H), 3.51–3.74 (m, 28 H), 3.42 (t, 2 H, J = 6.8 Hz), 3.04–3.20 (m, 2 H), 2.79 (t, 2 H, J = 7.2 Hz), 1.68 (quin, 2 H, J = 7.6 Hz), 1.55 (quin, 2 H, J = 7.0 Hz), 1.20–1.40 (m, 14 H). Mass analysis (MALDI-TOF): m/z 1022.6145 (calculated for $C_{54}H_{76}N_3O_{12}S_2$ $[M+H]^+$ m/z 1022.4865).

Synthesis of Fmoc-*L*-DOPS-7EG-PDS (6b).

Fmoc-*L*-DOPS-OH (94.4 mg, 0.22 mmol, 1.1 eq.) was coupled to 7EG-PDS **(5)** (122.6 mg, 0.21 mmol, 1 eq.) according to the general procedure described above. Then 76 mg of compound **6b** (37%) were obtained as a colorless oil. ^{1}H NMR (300 MHz, $CDCl_3$, 25 °C): *d* (ppm) = 8.47 (m, 1 H), 7.25–7.81 (m, 10 H), 7.06–7.15 (m, 2 H), 6.83 (d, 1 H, J = 7.9 Hz), 6.65 (d, 1 H, J = 7.9 Hz), 6.23 (br s, 1 H), 5.87 (br s, 1 H), 4.99 (m, 1 H), 4.46 (m, 2 H), 4.37 (m, 1 H), 4.24 (t, 1 H, J = 6.7 Hz), 3.48–3.78 (m, 28 H), 3.44 (t, 2 H, J = 7.0 Hz), 3.25 (m, 1 H), 2.80 (t, 2 H, J = 7.3 Hz), 1.63–1.79 (m, 2 H), 1.57 (quin, 2 H, J = 7.2 Hz), 1.22–1.42 (m, 14 H). Mass analysis (MALDI-TOF): m/z 1060.1505 (calculated for $C_{54}H_{75}N_3NaO_{12}S_2$ $[M+Na]^+$ m/z 1060.4634).

Synthesis of Fmoc-*L*-5-HTP-7EG-PDS (6c).

Fmoc-*L*-5-HTP-OH (140.7 mg, 0.32 mmol, 1.1 eq.) was coupled to 7EG-PDS compound **(5)** (179.5 mg, 0.29 mmol, 1 eq.) according to the general procedure described above. Then 133 mg of compound **6c** (44%) were obtained as a colorless oil. ^{1}H NMR (500 MHz, $CDCl_3$, 25 °C): *d* (ppm) = 8.73 (s, 1 H), 8.46 (m, 1 H), 7.19–7.80 (m, 12 H), 7.02–7.09 (m, 2 H), 6.80 (m, 1 H), 6.23 (br s, 1 H), 6.14 (br s, 1 H), 5.87 (m, 1 H), 4.35–4.50 (m, 3 H), 4.23 (t, 1 H, J = 7.1 Hz), 3.45–3.71 (m, 28 H), 3.42 (t, 2 H, J = 6.9 Hz), 3.16–3.40 (m, 1 H), 3.00–3.08 (m, 1 H), 2.78 (t, 2 H, J = 7.0 Hz), 1.68 (quin, 2 H, J = 7.3 Hz), 1.55 (quin, 2 H, J = 6.9 Hz), 1.19–1.41 (m, 14 H). Mass analysis (MALDI-TOF): m/z 1067.5042 (calculated for $C_{56}H_{76}N_4NaO_{11}S_2$ $[M+Na]^+$ m/z 1067.4844).

Synthesis of Fmoc-*L*-His-7EG-PDS (6d).

Fmoc-*L*-His(Trt)-OH (105.3 mg, 0.17 mmol, 1.1 eq.) was coupled to 7EG-PDS compound **(5)** (97.4 mg, 0.15 mmol, 1 eq.) according to the general procedure described above with a minor change. Before purification by column chromatography, the Trt protecting group was cleaved with 20% trifluoroacetic acid solution in DCM for 1 h at room temperature. The mixture was diluted with DCM, washed with saturated aqueous sodium bicarbonate (3 × eq. vol.), dried with magnesium sulfate, and then rotovapped to dryness. The compound was purified by silica gel chromatography (eluent: DCM/ethyl acetate 9:1 to 1:9 and DCM/MeOH 9:1). Then 56.3 mg of compound **6d** (37%) were obtained as a colorless oil. ^{1}H NMR (300 MHz, $CDCl_3$, 25 °C): *d* (ppm) = 8.46 (m, 1 H), 7.25–7.79 (m, 11 H), 7.07 (m, 1 H), 6.96 (m, 1 H), 6.55 (m, 1 H), 4.57 (m, 1 H), 4.32–4.41 (m, 2 H), 4.22 (t, 1 H, J = 7.1 Hz), 3.46–3.72 (m, 28 H), 3.41 (t, 2 H, J = 7.0 Hz), 3.00–3.34 (m, 2 H), 2.79 (t, 2 H, J = 7.1 Hz), 1.68 (quin, 2 H, J = 7.7 Hz), 1.54 (quin, 2 H, J = 6.6 Hz), 1.17–1.45 (m, 14 H). Mass analysis (MALDI-TOF): m/z 1002.4191 (calculated for $C_{51}H_{73}N_5NaO_{10}S_2$ $[M+Na]^+$ m/z 1002.4691).

Synthesis of Fmoc-*L*-Trp-7EG-PDS (6e).

Fmoc-*L*-Trp(Boc)-OH (106 mg, 0.20 mmol, 1 eq.) was coupled to 7EG-PDS compound **(5)** (125 mg, 0.20 mmol, 1 eq.) according to the general procedure described above with a minor change. Before purification by column chromatography, the Boc protecting group was cleaved with 20% TFA solution in DCM for 1 h at room temperature. The mixture was diluted with DCM, washed with saturated aqueous sodium bicarbonate (3× eq. vol.), dried with magnesium sulfate, and then rotovapped to dryness. The compound was purified by silica gel chromatography (eluent: DCM/ethyl acetate 9:1 to 1:9 and DCM/MeOH 9:1). Then 129 mg of compound **6e** (63%) were obtained as a colorless oil. ^{1}H NMR (500 MHz, $CDCl_3$, 25 °C): d (ppm) = 9.20 (s, 1 H), 8.45 (m, 1 H), 7.25–7.81 (m, 13 H), 7.04–7.21 (m, 2 H), 5.92 (m, 1 H), 5.83 (m, 1 H), 4.35–4.48 (m, 2 H), 4.23 (t, 1 H, J = 7.4 Hz), 3.45–3.75 (m, 28 H), 3.44 (t, 2 H, J = 6.8 Hz), 3.03–3.38 (m, 2 H), 2.78 (t, 2 H, J = 7.5 Hz), 1.68 (quin, 2 H, J = 7.5 Hz), 1.55 (quin, 2 H, 7.0 Hz) 1.18–1.42 (m, 14 H). Mass analysis (MALDI-TOF): m/z 1029.6008 (calculated for $C_{56}H_{77}N_4O_{10}S_2$ $[M+H]^+$ m/z 1029.5076).

General Procedure for the Coupling of Fmoc-Protected Neurotransmitter (Fmoc-R) to 7EG-PDS Compound (6).

Fmoc-R (1–1.1 eq.) was pre-activated in DCM or DMF (95–105 mM) with DIEA (3 eq.), HOBt (1.2 eq.), and EDC (1.2 eq.) for 30 min under argon. Thereafter, a 95 mM solution of compound **5** in DCM was added to the mixture. The solution was stirred for 24 h under argon at room temperature. The resultant mixture was diluted in DCM and washed with brine. The organic layer was dried with magnesium sulfate and then rotovapped to remove all remaining liquid. The compound was purified by silica gel chromatography (eluent: DCM/ethyl acetate 9:1 to 1:9 and DCM/MeOH 19:1).

Substrate Preparation and Chemical Lift-Off Lithography.

The Au substrates were hydrogen-flame annealed and then immersed in ethanolic solutions of 0.5 mM TEG for ~18 h for SAM formation. After self-assembly, substrates were rinsed with ethanol and blown dry with nitrogen gas. Polydimethylsiloxane (PDMS) stamps were prepared by thoroughly mixing a 10:1 mass ratio of *SYLGARD®* 184 silicone elastomer base and curing agent, respectively, in a plastic cup. Mixtures were degassed under vacuum to remove bubbles and cast onto photolithographically fabricated silicon master substrates situated in plastic Petri dishes. Elastomeric mixtures and silicon masters were baked at 70 °C in an oven for ~20 h. Polymerized PDMS stamps were removed from the masters and cut into smaller sizes for easy handling.

To prepare for lift-off lithography, PDMS stamps were exposed to oxygen plasma (power 18 W, oxygen pressure 10 psi, Harrick Plasma, Ithaca, NY, USA) for 40 s to generate reactive siloxyls on stamp surfaces.[9] Activated stamps were brought immediately into conformal contact with TEG-modified Au substrates for ~17 h. After stamp removal, post-lift-off substrates were rinsed thoroughly with ethanol. Preliminary experiments were carried out to investigate the effects of different incubation (insertion) times (0.25 h-24 h) using *L*-DOPA pre-functionalized thiols (Figure S1). Since fluorescence intensities were maximal and did not differ between the 3 h and 24 h time points, patterned substrates were submerged in

ethanolic solutions of 0.5 mM pre-functionalized thiols for 3 h for the remainder of the experiments in this study.

For post-functionalization, following lift-off, substrates were submerged in ethanolic solutions of 0.5 mM AEG for 3 h followed by on-substrate neurotransmitter conjugation. To vary the amounts of inserted pre-functionalized thiols or AEG, each was co-incubated in varying proportions with TEG such that total solution concentrations were 1.0 mM. After insertion, substrates were rinsed with ethanol and blown dry with nitrogen gas. Substrates with AEG tethers were incubated with 35 mM each small molecule, NHS, and EDC for 3 h. After post-functionalization, substrates were rinsed with ethanol and dried with nitrogen gas.

To pattern the same small-molecule probe by two different methods (*i.e.*, pre- *vs.* post-functionalization) on the same substrates, PDMS stamps were used to lift-off TEG SAM molecules twice.[9,10] After the first lift-off step, substrates were inserted with either AEG tethers or pre-functionalized thiols. For the second lift-off step, PDMS stamps were used to lift-off TEG SAM molecules from spatially non-overlapping regions adjacent to previously patterned regions on the same substrates. The double-lift-off substrates were then inserted with either pre-functionalized thiols or AEG tethers, respectively. For post-patterning functionalization, AEG was co-deposited with TEG at a 0.75 mole fraction for *L*-5-HTP and a 1.0 mole fraction for *L*-DOPA. In both cases, neurotransmitter conjugation was carried out immediately following the AEG insertion steps. For bi-functionalized substrates, lift-off lithography was performed twice as described except a different pre-functionalized thiol was inserted after each lift-off step.

The Fmoc groups used to protect amino moieties during chemical synthesis of pre-functionalized thiols or to provide protection from competing reactions during post-functionalization were removed after surface deposition by immersing substrates in 20% 4-methylpiperidine in deionized water for 15 min. After rinsing with deionized water, all neurotransmitter-modified substrates were incubated with 10 mg/mL BSA for 5 min to reduce nonspecific adsorption of target proteins.[2] Substrates were then completely submerged in deionized water in plastic Petri dishes and gently agitated. This step was repeated using fresh deionized water prior to exposing substrates to antibody solutions. Substrates were always covered with deionized water or antibody solutions. Keeping the substrates wet reduced the likelihood for captured antibodies to denature or to dissociate from substrates.

Antibody Binding.

Primary and secondary antibodies (Table S1) were diluted 1:200 and 1:100, respectively in 0.01 M PBS. Primary antibodies were incubated with substrates for 20 min, followed by incubation with fluorescently labeled secondary antibodies for 20 min at room temperature.[2] Substrates in plastic Petri dishes were incubated in the dark to reduce photobleaching of dye-labeled secondary antibodies. An inverted fluorescence microscope (Axio Observer.D1) equipped with an AxioCam MRm charged-coupled device camera was used to image substrates (Carl Zeiss MicroImaging, Inc., Thornwood, NY, USA). Two fluorescence filter sets, 38 HE/high efficiency with excitation and emission wavelengths of 470 ± 20 nm and 525 ± 25 nm, respectively, and 43 HE/high efficiency with excitation and emission

wavelengths of 550 ± 25 nm and 605 ± 70 nm, respectively, were used to visualize secondary antibody binding on substrates. Fluorescence images were collected using a 10× objective lens.

Fluorescence intensities were determined by performing line scans across patterned and unpatterned regions at a 30-pixel scanning width using AxioVs40 version 4.7.1.0 software (Carl Zeiss MicroImaging, Inc., Thornwood, NY, USA). On average, five line scans were acquired per substrate. All substrates from the same experiment were imaged using the same exposure times to standardize contrast and brightness. Fluorescence intensities were normalized to values for control (unpatterned) regions for each substrate and are reported as mean relative fluorescence units (RFU) (N=3 substrates per condition). Fluorescence images shown in the figures are those that most closely represented mean fluorescence intensities. For control experiments where primary antibodies were omitted, representative images were acquired using maximal exposure times to facilitate visualization.

X-ray Photoelectron Spectroscopy.

All X-ray photoelectron spectroscopy (XPS) data were collected using an AXIS Ultra DLD instrument (Kratos Analytical Inc., Chestnut Ridge, NY, USA). For XPS measurements, 100% pre-functionalized alkanethiols were self-assembled on Au substrates. A monochromatic Al K_α X-ray source (10 mA for survey scans and 20 mA for high resolution scans, 15 kV) with a 200-μm circular spot size and ultrahigh vacuum (10^{-9} Torr) were used.[5,9,28] Survey spectra were acquired at a pass energy of 160 eV using a 100 ms dwell time. High-resolution spectra of C 1s, O 1s, S 2p, N 1s, and Au 4f regions were acquired at a pass energy of 10 eV using a 200 ms dwell time. Different numbers of scans were carried out depending on the difficulty of identifying each peak *vs.* background, ranging from 5 to 30 scans. All XPS peaks for each element on Au substrates were referenced to the Au 4f signal at 84.0 eV. Atomic percentages were calculated from peak areas using CasaXPS version 2.3.16 software.

Electrochemistry.

A custom-made (polytetrafluoroethylene) electrochemical cell and a three-electrode setup were used with a Ag/AgCl reference electrode and a Pt-wire counter electrode. Functionalized substrates prepared as described above using featureless PDMS stamps for full surface target coverage were used as working electrodes. Top electrical contact was made using a machined gold ring; a rubber O-ring on the interior of the gold ring was used to make a leak-proof seal with each surface. The working electrode areas were 0.08 cm^2. Cyclic voltammetry measurements were made using a Reference 600 Potentiostat/Galvanostat/ZRA (Gamry Instruments, Warminster, PA, USA) and PHE200 Physical Electrochemistry Software (Gamry Instruments). Cyclic voltammograms were obtained at scan rates of 20, 40, 60, 80, and 100 mV/s. Nonlinear behavior was observed above 100 mV/s. All scans were from −400 mV to +800 mV, starting at 0 mV and were repeated ten times consecutively at each scan rate in deoxygenated tris-EDTA buffer. The first complete voltammogram at each scan rate was used for analysis due to diminishing peak currents with subsequent scans within the same run.

Surface densities of pre- and post-functionalized thiols were calculated using the following equation:

$$\Gamma = \frac{4i_p RT}{n^2 F^2 vA}$$

where Γ is the molecule surface density (moles/cm^2), ip is the anodic peak current (A), R is the universal gas constant, T is the absolute temperature, n is the number electrons (2), F is Faraday's constant, v is the scan rate (V/s), and A is the electrode area (cm^2). Surface densities were calculated at each scan rate and averaged across scan rates to give a mean value for each sample. The experimenter that conducted electrochemical measurements was blind to outcomes of the fluorescence measurements.

Statistics.

Differences in relative fluorescence data were evaluated by one-way analysis of variance followed by Tukey's *post hoc* tests (multiple comparisons) or Student's *t*-tests (two-group comparisons) using Prism Version 5.02 (GraphPad Software Inc., San Diego, USA). Relative fluorescence intensities are reported as means ± standard errors of the means with probabilities $P<0.05$ considered statistically significant.

RESULTS AND DISCUSSION

Synthesis of Pre-Functionalized Thiols.

The availability of functional oligo(ethylene glycol)-terminated alkanethiols is limited and none of the molecules needed for this study were commercially available. Thus, we devised and performed synthesis as shown in Scheme 1. Hepta(ethylene glycol) was monoetherified with 11-bromo-1-undecene. A large excess of hepta(ethylene glycol) was used to favor monosubstitution,[29] because a stoichiometric equivalent of both reagents generally yielded a statistical proportion of unmodified, mono-, and disubstituted molecules. Monoetherification was achieved according to an established protocol[27] using a three-fold excess of hepta(ethylene glycol) compared to 11-bromo-1-undecene with a slight excess of 50% sodium hydroxide to give compound **1** in 63% yield. The terminal olefin then underwent a photoinitiated thiol-ene reaction with thioacetic acid in the presence of AIBN to give compound **2** in good yield (91%). The terminal alcohol was converted to a tosylate leaving group (compound **3**), which was subsequently reacted with sodium azide to provide compound **4** with a yield of 94%.

The terminal azide group was reduced to a primary amine using triphenylphosphine, which also cleaved the thioacetate. The resulting free thiol was then protected with 2,2'-dithiodipyridine (2-PDS) to give compound **5** with an overall yield of 45%. The pyridyl disulfide (PDS) moieties protected thiols from dimerization and other side reactions during the neurotransmitter coupling procedures. The PDS protecting groups were used because of their selectivity toward thiols and their reactivity with Au surfaces.[30] Finally, the terminal amine was coupled to Fmoc-R to form an amide bond using standard coupling agents (HOBt and EDC in the presence of DIEA). The side-chain protecting groups of *L*-His and *L*-Trp,

trityl (Trt) and *tert*-butyloxycarbonyl (Boc) groups, respectively, were removed with 20% TFA in DCM. The final pre-functionalized thiols (Fmoc-R-7EG-PDS) were obtained in 37–63% yields depending on the neurotransmitter R-group. X-ray photoelectron spectroscopy was used to determine self-assembly of *L*-DOPA and *L*-5-HTP pre-functionalized thiols on Au surfaces (Table S2 and Figure S2).

Although there are literature reports of the synthesis of oligo(ethylene glycol)-terminated alkanethiols,[27,29,31,32] few studies have reported on pre-functionalization of these tethers with biologically active small molecules.[33–36] To the best of our knowledge, pre-functionalization with neurotransmitters or their precursors has not been reported.

Patterning Pre- *vs.* Post-Functionalized Thiols with Lift-Off Lithography.

Chemical lift-off lithography was used to pattern TEG SAMs, which functioned as biomolecule-resistant background matrices (Figure 1B). Following lithography, which removes ~70% of TEG in the contact regions,[9,17,28,37] pre-functionalized thiols were inserted into the lift-off regions (Figure 1C). For post-functionalization, AEG tethers were inserted into the lift-off regions. Functionalization with Fmoc-protected neurotransmitters (Fmoc-R) *via* amide bond formation was then carried out directly on substrates.[2,3] Prior to antibody binding, Fmoc protecting groups were removed from pre- and post-functionalized thiols to reveal epitopes needed for molecular recognition.

Oxygen plasma-treated PDMS stamps patterned with 25 × 25 μm^2 square-shaped protruding features separated by 25 μm spacings were used for lift-off lithography.[9,10] Because SAM molecules are removed only in the stamp-contact regions, patterns of negative, recessed squares were created on Au surfaces. Lifted-off substrates were exposed to varying mole fractions of TEG and pre-functionalized thiols, or TEG and AEG tether molecules followed by post-functionalization. The goal of these experiments was to determine antibody recognition as a function of insertion compositions.

Following patterning, insertion, and surface functionalization (post-functionalized thiols), primary antibodies against each probe were captured on substrates. Primary antibody binding was visualized *via* capture of fluorescently labeled secondary antibodies (Table S1). Fluorescent square patterns against dark biomolecule-resistant TEG backgrounds resulted from antibody capture (Figure 2). As nominal solution mole fractions of *L*-DOPA or *L*-5-HTP pre-functionalized thiols increased relative to TEG, fluorescence intensities increased slowly. Large increases in fluorescence intensities occurred at 100% pre-functionalized thiols (Figure 2A,B left to right). Substrates exposed to fluorescently labeled secondary antibodies in the absence of primary antibodies showed negligible fluorescence indicating minimal secondary antibody recognition of *L*-DOPA or *L*-5-HTP pre-functionalized thiols (Figure S3A,B).

We hypothesized that fluorescence intensities would increase proportionally with increasing fractions of pre-functionalized thiols. We assumed that fluorescence quenching is minimal. Chemical lift-off of TEG in the contact regions is incomplete;[9,17] the remaining TEG molecules act as “spacers” diluting inserted molecules and preventing quenching due to poor orientation or fluorophore packing.[28] Others have shown that dilution with alkanethiols

minimizes quenching by orienting probes away from Au substrates.[38,39] Further, low-density probe environments improve recognition by providing better target access.[40–42]

Contrary to our hypothesis, however, fluorescence signals did not linearly increase with increasing fractions of pre-functionalized thiols (Figure 3A,B). Factors likely to contribute to this behavior include differences in the relative rates of diffusion of different molecules to surfaces[43] and differences in thiol miscibility[44] (*i.e.*, pre-functionalized thiols may be less miscible with TEG remaining in the lift-off regions). Importantly, pyridyl disulfides are bulkier than thiols and require cleavage upon adsorption on Au substrates.[30,45] Studies by others on competitive adsorption have shown that adsorption of thiols is about two orders of magnitude faster than disulfides.[46,47] In sum, these results demonstrate that co-incubation with TEG is not necessary for maximal insertion and recognition of pre-functionalized thiols; the TEG molecules remaining in the lift-off regions appear to provide the dilution needed to achieve maximal antibody binding.

Similar patterning and antibody capture were carried out in conjunction with post-functionalization (Figure 2C,D). Behavior with respect to nominal AEG tether/TEG mole fractions was different from that observed with pre-functionalized thiols (Figure 2A,B). For post-functionalizaton, fluorescence intensities increased at low AEG proportions, quickly approaching maxima for both *L*-DOPA and *L*-5-HTP (Figure 3C,D). Similar to pre-functionalized substrates, negligible secondary antibody recognition of substrates post-functionalized with *L*-DOPA or *L*-5-HTP was observed (Figure S3C,D).

For post-functionalized thiols, neurotransmitters were conjugated to surface tethers inserted into lift-off regions. In this case, antibody binding depends on surface tether densities and the efficiency of the NHS/EDC coupling chemistry in attaching *L*-DOPA or *L*-5-HTP to substrates, among other factors. Unlike pre-functionalized thiols, AEG tethers do not possess bulky Fmoc-protected neurotransmitters or pyridyl disulfides. Since AEG tethers resemble TEG more closely than do pre-functionalized thiols (Figure 1A), insertion of AEG is likely to follow solution molar ratios more closely. At χ=1, molecular crowding may come into play, even with the dilution provided by the TEG remaining after lift-off. Tether crowding could affect probe functionalization yields and/or target recognition. We note that the pre-functionalized strategy consistently resulted in smaller substrate-to-substrate variations as evidenced by smaller errors for replicate determinations compared to post-functionalization at all mole fractions tested (Figure 3).

Side-by-Side Comparisons of Pre- *vs.* Post-functionalized Approaches.

To investigate directly the idea that pre-functionalizing small molecules to surface tethers prior to self-assembly improves biomolecule recognition, we compared pre- *vs.* post-functionalization approaches on the same substrates. Lift-off lithography was carried out twice on each substrate, resulting in two possible patterning routes. In the first, neurotransmitter pre- functionalized thiols were inserted into lift-off regions, followed by a second lift-off step in an adjacent region, insertion of AEG tethers, and post-functionalization (*i.e.*, pre-functionalization followed by post-functionalization) (Figure 4A). The second route involved inserting AEG tethers into lift-off regions followed by probe conjugation. Another lift-off step was performed in an adjacent substrate region and

neurotransmitter pre-functionalized thiols were inserted into the newly lifted-off areas (*i.e.*, post-functionalization followed by pre-functionalization) (Figure S4A).

Relative fluorescence intensities for *L*-DOPA pre- *vs.* post-functionalized thiols were similar, regardless of the patterning route (Figure 4B,D, Figure S4B,D). In contrast, *L*-5-HTP relative fluorescence intensities were higher for pre- *vs.* post-functionalized thiols for both patterning routes (Figure 4C,D, Figure S4C,D). Capture surfaces exposed to secondary antibodies alone showed negligible fluorescence patterns regardless of patterning order (Figure S5). These findings suggest that while pre-functionalized thiols can be used to increase biomolecule recognition of tethered small molecules, improvements depend on specific probes.

Characterization of Probe Surface Densities.

Probe-specific differences in biomolecule capture for pre- *vs.* post-functionalized immobilization prompted investigation of densities of surface-tethered *L*-DOPA and *L*-5-HTP, which were determined by cyclic voltammetry (Figure 5A,B). Anodic peaks (100—150 mV *vs.* Ag/AgCl) indicative of two-electron oxidation of *L*-DOPA or *L*-5-HTP (Figure 5C) were used for analysis. No signal in this region was detected for control substrates where AEG was inserted into post-lift-off regions *sans* surface chemistry to tether probes. Cathodic peaks overlapped with changes in current from control substrates and thus, these peaks were not analyzed.

Anodic peak current values were plotted as a function of scan rate (Figure S6). Linear relationships indicated that *L*-DOPA and *L*-5-HTP were covalently bound to substrates *via* both immobilization strategies (as opposed to being transiently adsorbed). Surface densities are shown in Figure 5D. The densities of *L*-DOPA in the pre- *vs.* post-functionalized conditions were comparable, whereas higher densities of *L*-5-HTP were determined for pre- *vs.* post-functionalized substrates. Differences in probe surface densities correlated with antibody capture for *L*-5-HTP (significant differences) and *L*-DOPA (no significant differences) pre- *vs.* post-functionalized substrates (Figure 4D, Figure S4D).

Doubly Patterned Pre-Functionalized Substrates.

Pre-functionalized thiols circumvent the need for sequential and compatible on-substrate coupling chemistries. We investigated the use of pre-functionalized thiols to create substrates patterned with two different neurotransmitters. This capability enables the preparation of multiplexed substrates for side-by-side binding comparisons, on-chip control experiments, and separations of biologically active molecules.[2,3,5]

Side-by-side double-lift-off lithography was used to pattern *L*-DOPA and *L*-5-HTP pre-functionalized thiols on the same substrates. Substrates were exposed to primary antibody solutions containing both anti-*L*-DOPA and anti-*L*-5-HTP antibodies. Primary antibody binding was visualized *via* exposure to solutions containing AlexaFluor® 488 (peak emission at 519 nm; “green”) and AlexaFluor® 546 (peak emission at 573 nm; “red”) secondary antibodies (Table S1). We hypothesized that primary and secondary antibodies would sort to their respective binding partners so that *L*-DOPA patterned regions would be

labeled with green fluorescence and *L*-5-HTP patterned regions would be labeled with red fluorescence.

We found that anti-*L*-DOPA antibodies selectively recognized surface-tethered *L*-DOPA *vs.* *L*-5-HTP (Figure 6A-C). However, anti-*L*-5-HTP antibodies did not distinguish surface-tethered *L*-5-HTP from *L*-DOPA (Figure 6D-F). Substrates exposed to fluorescently labeled secondary antibodies alone displayed negligible fluorescence (Figure S7A-D). Because variabilities in the extents of probe functionalization and side reactions, which affect specific antibody binding, were avoided through the use of pre-functionalized thiols, anti-*L*-5-HTP antibodies likely cross-reacted with *L*-DOPA because of the properties of these particular antibodies.[51,52]

Poor antibody specificity was evident for other pairs of neurotransmitter pre-functionalized thiols on doubly patterned substrates. For example, anti-*L*-DOPA antibodies selectively recognized *L*-DOPA *vs.* *L*-His (Figure 7A-C) or *L*-Trp (Figure 7D-F). By contrast, both anti-*L*-His and anti-*L*-Trp antibodies failed to display selective recognition of *L*-His (Figure S8A-C) or *L*-Trp (Figure S8D-F). In fact, the latter antibodies showed greater fluorescence intensities for the wrong target (*i.e.,* *L*-DOPA). Anti-*L*-DOPA antibodies did not significantly distinguish *L*-DOPA *vs.* *L*-DOPS (Figure 7G-I). This pair of probes is the most difficult to differentiate of the substrate pairs investigated as *L*-DOPA and *L*-DOPS differ by a single hydroxyl group (Figure 1A).[53,54] In all cases, negligible fluorescence was associated with secondary antibody binding in the absence of primary antibodies (Figure S9A-J). We could not identify commercially available antibodies for *L*-DOPS, so experiments focused on differentiating *L*-DOPS from *L*-DOPA could not be performed.

In our previous work using post-functionalization, we found that primary antibodies for small molecules exhibited significant cross-reactivity.[2] At that time, we did not have access to pre-functionalized thiols, so we could not rule out the possibility that incomplete surface functionalization contributed to antibody cross-reactivity. Hence, one motivation for the present study was to investigate cross-reactivity using the pre-functionalization strategy. However, even when using pre-functionalized thiols to produce bi-functional substrates, we continued to observe significant cross-reactivities (Figures 6, 7, and S8).

In the present study, we used the only antibodies publicly available for the small-molecule probes investigated. Monoclonal antibodies were not available for most probes with the exception of *L*-DOPA, where polyclonal antibodies were not available. For the other small-molecule probes, *i.e.,* *L*-5-HTP, *L*-His, *L*-Trp, and *L*-DOPS, only polyclonal antibodies were commercially available. Monoclonal antibodies are identical and recognize the same epitope on an antigen. Polyclonal antibodies are polydisperse, recognizing different epitopes on antigens.[55] As such, polyclonal antibodies are more susceptible to cross-reactivity.[24] The findings in Figures 6, 7, and S8 are consistent with the literature on differences in cross-reactivity between monoclonal and polyclonal antibodies.[56] Moreover, antibodies in general are known to be fraught with problems associated with selectivity.[57]

CONCLUSIONS AND PROSPECTS

We describe the synthesis of monodisperse oligo(ethylene glycol)-terminated alkanethiols pre-functionalized with neurotransmitter precursors. This synthetic route offers several advantages. First, it enables heterobifunctional tethers to be produced that are otherwise not commercially available. Second, it permits orthogonal coupling chemistries that preserve the integrity of small-molecule probe functional groups. Third, conjugation of a number of different neurotransmitter precursors demonstrates the versatility of this strategy, which should be applicable to other small-molecule probes.

Pre-functionalized thiols enabled head-to-head comparisons with post-functionalized thiols in the context of biorecognition. Pre-functionalized thiols withstood subsequent conditions associated with additional on-substrate chemistries. While biorecognition was more consistent for pre-functionalized thiols, we determined that on-substrate functionalization, for the specific probes tested, also worked well. Differences between on-substrate functionalization and pre-functionalization depended on specific probes. While pre-functionalized thiols may present a more reliable option for small-molecule recognition, for large arrays containing many different probes, synthesis of pre-functionalized alkanethiols may be limiting.

When it comes to finding a solution to cross-reactivity associated with biomolecule targets, improving specific recognition *via* careful control of surface chemistries appears to be insufficient. That is, the present findings indicate that a remaining fundamental limitation lies with the biomolecule binding partners themselves; in this case, antibodies that failed to discriminate small-molecule probes on chemically defined surfaces. Binding partners, such as engineered cellular receptors[53,58] or synthetic oligonucleotides, *i.e.*, aptamers, may be advantageous.[59–62] Aptamers are chemically synthesized. Their structures are identical and affinities can be tuned by modifying oligonucleotide sequences and thus, binding conformations.[63] Pre-functionalized thiols and chemical patterning strategies with multiplexing capabilities will facilitate fabrication of improved small-molecule functionalized substrates for identifying highly specific biomolecule binding partners. The latter can be incorporated into biosensing platforms for detecting neurotransmitters and other important small-molecules.[63–67]

ASSOCIATED CONTENT

Supplementary Material

Refer to Web version on PubMed Central for supplementary material.

ACKNOWLEDGMENTS

This work was supported by the U.S. Department of Energy (DE-SC-1037004), the National Institutes of Health (DP2-OD008533), the National Institute on Drug Abuse (DA045550), the California Neurotechnologies Program, and the Kavli Foundation. The authors wish to thank Mr. George Major for assistance with electrochemical experiments, Dr. Andrew Serino for assistance with XPS, Prof. Wei-Ssu Liao for helpful discussions, and Prof. Andre Nel for fluorescence microscope use.

REFERENCES

(1.) Shuster MJ; Vaish A; Gilbert ML; Martinez-Rivera M; Nezarati RM; Weiss PS; Andrews AM Comparison of Oligo(Ethylene Glycol)Alkanethiols *versus N*-Alkanethiols: Self-Assembly, Insertion, and Functionalization. J. Phys. Chem. C 2011, 115, 24778–24787.

2.) Liao WS; Cao HH; Cheunkar S; Shuster MJ; Altieri SC; Weiss PS; Andrews AM Small-Molecule Arrays for Sorting G-Protein-Coupled Receptors. J. Phys. Chem. C 2013, 117, 22362–22368.

3.) Shuster MJ; Vaish A; Cao HH; Guttentag AI; McManigle JE; Gibb AL; Martinez MM; Nezarati RM; Hinds JM; Liao WS; Weiss PS; Andrews AM Patterning Small-Molecule Biocapture Surfaces: Microcontact Insertion Printing *vs.* Photolithography. Chem. Commun 2011, 47, 10641–10643.

4.) Vaish A; Shuster MJ; Cheunkar S; Singh YS; Weiss PS; Andrews AM Native Serotonin Membrane Receptors Recognize 5-Hydroxytryptophan-Functionalized Substrates: Enabling Small-Molecule Recognition. ACS Chem. Neuro 2010, 1, 495–504.

5.) Vaish A; Shuster MJ; Cheunkar S; Weiss PS; Andrews AM Tuning Stamp Surface Energy for Soft Lithography of Polar Molecules to Fabricate Bioactive Small-Molecule Microarrays. Small 2011, 7, 1471–1479. [PubMed: 21538866]

6.) Shuster MJ; Vaish A; Szapacs ME; Anderson ME; Weiss PS; Andrews AM Biospecific Recognition of Tethered Small Molecules Diluted in Self-Assembled Monolayers. Adv. Mater 2008, 20, 164–167.

7.) Mullen TJ; Srinivasan C; Hohman JN; Gillmor SD; Shuster MJ; Horn MW; Andrews AM; Weiss PS Microcontact Insertion Printing. Appl. Phys. Lett 2007, 90, 1–3.

8.) Saavedra HM; Mullen TJ; Zhang PP; Dewey DC; Claridge SA; Weiss PS Hybrid Strategies in Nanolithography. Rep. Prog. Phys 2010, 73, 1–40.

9.) Liao WS; Cheunkar S; Cao HH; Bednar HR; Weiss PS; Andrews AM Subtractive Patterning *via* Chemical Lift-Off Lithography. Science 2012, 337, 1517–1521. [PubMed: 22997333]

10.) Andrews AM; Liao WS; Weiss PS Double-Sided Opportunities Using Chemical Lift-Off Lithography. Acc. Chem. Res 2016, 49, 1449–1457. [PubMed: 27064348]

11.) Bumm LA; Arnold JJ; Cygan MT; Dunbar TD; Burgin TP; Jones L; Allara DL; Tour JM; Weiss PS Are Single Molecular Wires Conducting? Science 1996, 271, 1705–1707.

12.) Cygan MT; Dunbar TD; Arnold JJ; Bumm LA; Shedlock NF; Burgin TP; Jones L; Allara DL; Tour JM; Weiss PS Insertion, Conductivity, and Structures of Conjugated Organic Oligomers in Self-Assembled Alkanethiol Monolayers on Au{111}. J. Am. Chem. Soc 1998, 120, 2721–2732.

13.) Claridge SA; Liao WS; Thomas JC; Zhao YX; Cao HH; Cheunkar S; Serino AC; Andrews AM; Weiss PS From the Bottom Up: Dimensional Control and Characterization in Molecular Monolayers. Chem. Soc. Rev 2013, 42, 2725–2745. [PubMed: 23258565]

14.) Spinke J; Liley M; Guder HJ; Angermaier L; Knoll W Molecular Recognition at Self-Assembled Monolayers - the Construction of Multicomponent Multilayers. Langmuir 1993, 9, 1821–1825.

15.) Ostuni E; Yan L; Whitesides GM The Interaction of Proteins and Cells with Self-Assembled Monolayers of Alkanethiolates on Gold and Silver. Colloids Surf. B 1999, 15, 3–30.

16.) Harder P; Grunze M; Dahint R; Whitesides GM; Laibinis PE Molecular Conformation in Oligo(Ethylene Glycol)-Terminated Self-Assembled Monolayers on Gold and Silver Surfaces Determines Their Ability to Resist Protein Adsorption. J. Phys. Chem. B 1998, 102, 426–436.

17.) Cao HH; Nakatsuka N; Liao WS; Serino AC; Cheunkar S; Yang HY; Weiss PS; Andrews AM Advancing Biocapture Substrates *via* Chemical Lift-Off Lithography. Chem. Mater 2017, 29, 6829–6839.

18.) Sam S; Touahir L; Andresa JS; Allongue P; Chazalviel JN; Gouget-Laemmel AC; de Villeneuve CH; Moraillon A; Ozanam F; Gabouze N; Djebbar S Semiquantitative Study of the EDC/NHS Activation of Acid Terminal Groups at Modified Porous Silicon Surfaces. Langmuir 2010, 26, 809–814. [PubMed: 19725548]

19.) Wang C; Yan Q; Liu HB; Zhou XH; Xiao SJ Different EDC/NHS Activation Mechanisms between PAA and PMAA Brushes and the Following Amidation Reactions. Langmuir 2011, 27, 12058–12068. [PubMed: 21853994]

20.) Xia N; Xing Y; Wang GF; Feng QQ; Chen QQ; Feng HM; Sun XL; Liu L Probing of EDC/NHSS-Mediated Covalent Coupling Reaction by the Immobilization of Electrochemically Active Biomolecules. Int. J. Electrochem. Sc 2013, 8, 2459–2467.
21.) Collman JP; Devaraj NK; Eberspacher TPA; Chidsey CED Mixed Azide-Terminated Monolayers: A Platform for Modifying Electrode Surfaces. Langmuir 2006, 22, 2457–2464. [PubMed: 16519441]
22.) Bumm LA; Arnold JJ; Charles LF; Dunbar TD; Allara DL; Weiss PS Directed Self-Assembly to Create Molecular Terraces with Molecularly Sharp Boundaries in Organic Monolayers. J. Am. Chem. Soc 1999, 121, 8017–8021.
23.) Saavedra HM; Thompson CM; Hohman JN; Crespi VH; Weiss PS Reversible Lability by *in Situ* Reaction of Self-Assembled Monolayers. J. Am. Chem. Soc 2009, 131, 2252–2259. [PubMed: 19170497]
24.) Stranick SJ; Parikh AN; Tao YT; Allara DL; Weiss PS Phase-Separation of Mixed-Composition Self-Assembled Monolayers into Nanometer-Scale Molecular Domains. J. Phys. Chem 1994, 98, 7636–7646.
25.) Congreve M; Langmead CJ; Mason JS; Marshall FH Progress in Structure Based Drug Design for G Protein-Coupled Receptors. J. Med. Chem 2011, 54, 4283–4311. [PubMed: 21615150]
26.) Seeber M; De Benedetti PG; Fanelli F Molecular Dynamics Simulations of the Ligand-Induced Chemical Information Transfer in the 5-HT_{1A} Receptor. J. Chem. Inf. Comp. Sci 2003, 43, 1520–1531.
27.) Palegrosdemange C; Simon ES; Prime KL; Whitesides GM Formation of Self-Assembled Monolayers by Chemisorption of Derivatives of Oligo(Ethylene Glycol) of Structure $HS(CH_2)_{11}(OCH_2CH_2)_m$-OH on Gold. J. Am. Chem. Soc 1991, 113, 12–20.
28.) Cao HH; Nakatsuka N; Serino AC; Liao WS; Cheunkar S; Yang HY; Weiss PS; Andrews AM Controlled DNA Patterning by Chemical Lift-Off Lithography: Matrix Matters. ACS Nano 2015, 9, 11439–11454. [PubMed: 26426585]
29.) Svedhem S; Hollander CA; Shi J; Konradsson P; Liedberg B; Svensson SCT Synthesis of a Series of Oligo(Ethylene Glycol)-Terminated Alkanethiol Amides Designed to Address Structure and Stability of Biosensing Interfaces. J. Org. Chem 2001, 66, 4494–4503. [PubMed: 11421767]
30.) Vazquez-Dorbatt V; Tolstyka ZP; Chang CW; Maynard HD Synthesis of a Pyridyl Disulfide End-Functionalized Glycopolymer for Conjugation to Biomolecules and Patterning on Gold Surfaces. Biomacromolecules 2009, 10, 2207–2212. [PubMed: 19606855]
31.) Prime KL; Whitesides GM Adsorption of Proteins onto Surfaces Containing End-Attached Oligo(Ethylene Oxide) − A Model System Using Self-Assembled Monolayers. J. Am. Chem. Soc 1993, 115, 10714–10721.
32.) Tolstyka ZP; Richardson W; Bat E; Stevens CJ; Parra DP; Dozier JK; Distefano MD; Dunn B; Maynard HD Chemoselective Immobilization of Proteins by Microcontact Printing and Bio-Orthogonal Click Reactions. Chembiochem 2013, 14, 2464–2471. [PubMed: 24166802]
33.) Booth C; Bushby RJ; Cheng YL; Evans SD; Liu QY; Zhang HL Synthesis of Novel Biotin Anchors. Tetrahedron 2001, 57, 9859–9866.
34.) Kleinert M; Rockendorf N; Lindhorst TK Glyco-SAMs as Glycocalyx Mimetics: Synthesis of *L*-Fucose- and D-Mannose-Terminated Building Blocks. Eur. J. Org. Chem 2004, 3931–3940.
35.) Prats-Alfonso E; Oberhansl S; Lagunas A; Martinez E; Samitier J; Albericio F Effective and Versatile Strategy for the Total Solid-Phase Synthesis of Alkanethiols for Biological Applications. Eur. J. Org. Chem 2013, 1233–1239.
36.) Murray J; Nowak D; Pukenas L; Azhar R; Guillorit M; Walti C; Critchley K; Johnson S; Bon RS Solid Phase Synthesis of Functionalised SAM-Forming Alkanethiol-Oligoethyleneglycols. J. Mater. Chem. B 2014, 2, 3741–3744. [PubMed: 25400934]
37.) Slaughter LS; Cheung KM; Kaappa S; Cao HH; Yang Q; Young TD; Serino AC; Malola S; Olson JM; Link S; Hakkinen H; Andrews AM; Weiss PS Patterning of Supported Gold Monolayers *via* Chemical Lift-Off Lithography. Beilstein J. Nanotechnol 2017, 8, 2648–2661. [PubMed: 29259879]
38.) Arinaga K; Rant U; Tornow M; Fujita S; Abstreiter G; Yokoyama N The Role of Surface Charging During the Coadsorption of Mercaptohexanol to DNA Layers on Gold: Direct

Observation of Desorption and Layer Reorientation. Langmuir 2006, 22, 5560–5562. [PubMed: 16768474]

39.) Rant U; Arinaga K; Fujita S; Yokoyama N; Abstreiter G; Tornow M Structural Properties of Oligonucleotide Monolayers on Gold Surfaces Probed by Fluorescence Investigations. Langmuir 2004, 20, 10086–10092. [PubMed: 15518498]
40.) Josephs EA; Ye T Nanoscale Spatial Distribution of Thiolated DNA on Model Nucleic Acid Sensor Surfaces. ACS Nano 2013, 7, 3653–3660. [PubMed: 23540444]
41.) Murphy JN; Cheng AKH; Yu HZ; Bizzotto D On the Nature of DNA Self-Assembled Monolayers on Au: Measuring Surface Heterogeneity with Electrochemical in Situ Fluorescence Microscopy. J. Am. Chem. Soc 2009, 131, 4042–4050. [PubMed: 19254024]
42.) Josephs EA; Ye T Electric-Field Dependent Conformations of Single DNA Molecules on a Model Biosensor Surface. Nano Lett 2012, 12, 5255–5261. [PubMed: 22963660]
43.) Stranick SJ; Parikh AN; Allara DL; Weiss PS A New Mechanism for Surface-Diffusion − Motion of a Substrate-Adsorbate Complex. J. Phys. Chem 1994, 98, 11136–11142.
44.) Kakiuchi T; Iida M; Gon N; Hobara D; Imabayashi S; Niki K Miscibility of Adsorbed 1-Undecanethiol and 11-Mercaptoundecanoic Acid Species in Binary Self-Assembled Monolayers on Au(111). Langmuir 2001, 17, 1599–1603.
45.) Zareie HM; Boyer C; Bulmus V; Nateghi E; Davis TP Temperature-Responsive Self-Assembled Monolayers of Oligo(Ethylene Glycol): Control of Biomolecular Recognition. ACS Nano 2008, 2, 757–765. [PubMed: 19206608]
46.) Bain CD; Troughton EB; Tao YT; Evall J; Whitesides GM; Nuzzo RG Formation of Monolayer Films by the Spontaneous Assembly of Organic Thiols from Solution onto Gold. J. Am. Chem. Soc 1989, 111, 321–335.
47.) Bain CD; Biebuyck HA; Whitesides GM Comparison of Self-Assembled Monolayers on Gold − Coadsorption of Thiols and Disulfides. Langmuir 1989, 5, 723–727.
48.) Chan EWL; Yousaf MN Immobilization of Ligands with Precise Control of Density to Electroactive Surfaces. J. Am. Chem. Soc 2006, 128, 15542–15546. [PubMed: 17132022]
49.) Houseman BT; Gawalt ES; Mrksich M Maleimide-Functionalized Self-Assembled Monolayers for the Preparation of Peptide and Carbohydrate Biochips. Langmuir 2003, 19, 1522–1531.
50.) Duan CM; Meyerhoff ME Separation-Free Sandwich Enzyme Immunoassays Using Microporous Gold Electrodes and Self-Assembled Monolayer Immobilized Capture Antibodies. Anal. Chem 1994, 66, 1369–1377. [PubMed: 8017631]
51.) Prager EM The Sequence Immunology Correlation Revisited − Data for Cetacean Myoglobins and Mammalian Lysozymes. J. Mol. Evol 1993, 37, 408–416. [PubMed: 8308908]
52.) Benjamin DC; Berzofsky JA; East IJ; Gurd FRN; Hannum C; Leach SJ; Margoliash E; Michael JG; Miller A; Prager EM; Reichlin M; Sercarz EE; Smithgill SJ; Todd PE; Wilson AC The Antigenic Structure of Proteins − A Reappraisal. Annu. Rev. Immunol 1984, 2, 67–101. [PubMed: 6085753]
53.) Lacin E; Muller A; Fernando M; Kleinfeld D; Slesinger PA Construction of Cell-Based Neurotransmitter Fluorescent Engineered Reporters (CNiFERs) for Optical Detection of Neurotransmitters *in Vivo*. J. Vis. Exp 2016, 1–22.
54.) Nakatsuka N; Andrews AM Differentiating Siblings: The Case of Dopamine and Norepinephrine. ACS Chem. Neuro 2017, 8, 218–220.
55.) Lipman NS; Jackson LR; Trudel LJ; Weis-Garcia F Monoclonal *versus* Polyclonal Antibodies: Distinguishing Characteristics, Applications, and Information Resources. ILAR J 2005, 46, 258–268. [PubMed: 15953833]
56.) Benjamin DC; Berzofsky JA; East IJ; Gurd FR; Hannum C; Leach SJ; Margoliash E; Michael JG; Miller A; Prager EM; Reichlin M; Sercarz EE; Smithgill SJ; Todd PE; Wilson AC The Antigenic Structure of Proteins: A Reappraisal. Annu. Rev. Immunol 1984, 2, 67–101. [PubMed: 6085753]
57.) Baker M Reproducibility Crisis: Blame It on the Antibodies. Nature 2015, 521, 274–276. [PubMed: 25993940]
58.) Muller A; Joseph V; Slesinger PA; Kleinfeld D Cell-Based Reporters Reveal *in Vivo* Dynamics of Dopamine and Norepinephrine Release in Murine Cortex. Nat. Methods 2014, 11, 1245–1252. [PubMed: 25344639]

59.) McKeague M; Derosa MC Challenges and Opportunities for Small Molecule Aptamer Development. J Nucleic Acids 2012, 2012, 748913. [PubMed: 23150810]

60.) Kim YS; Gu MB Advances in Aptamer Screening and Small Molecule Aptasensors. Adv Biochem Eng Biotechnol 2014, 140, 29–67. [PubMed: 23851587]

61.) Mei H; Bing T; Yang X; Qi C; Chang T; Liu X; Cao Z; Shangguan D Functional-Group Specific Aptamers Indirectly Recognizing Compounds with Alkyl Amino Group. Anal Chem 2012, 84, 7323–7329. [PubMed: 22881428]

62.) Nakatsuka N; Cao HH; Deshayes S; Melkonian AL; Kasko AM; Weiss PS; Andrews AM Aptamer Recognition of Multiplexed Small-Molecule-Functionalized Substrates. In Revision 2018.

63.) Vallee-Belisle A; Plaxco KW Structure-Switching Biosensors: Inspired by Nature. Curr. Opin. Struc. Biol 2010, 20, 518–526.

64.) Kim J; Rim YS; Chen HJ; Cao HH; Nakatsuka N; Hinton HL; Zhao CZ; Andrews AM; Yang Y; Weiss PS Fabrication of High-Performance Ultrathin In_2O_3 Film Field-Effect Transistors and Biosensors Using Chemical Lift-Off Lithography. ACS Nano 2015, 9, 4572–4582. [PubMed: 25798751]

65.) Alivisatos AP; Andrews AM; Boyden ES; Chun M; Church GM; Deisseroth K; Donoghue JP; Fraser SE; Lippincott-Schwartz J; Looger LL; Masmanidis S; McEuen PL; Nurmikko AV; Park H; Peterka DS; Reid C; Roukes ML; Scherer A; Schnitzer M; Sejnowski TJ; Shepard KL; Tsao D; Turrigiano G; Weiss PS; Xu C; Yuste R; Zhuang XW Nanotools for Neuroscience and Brain Activity Mapping. ACS Nano 2013, 7, 1850–1866. [PubMed: 23514423]

66.) Biteen JS; Blainey PC; Cardon ZG; Chun MY; Church GM; Dorrestein PC; Fraser SE; Gilbert JA; Jansson JK; Knight R; Miller JF; Ozcan A; Prather KA; Quake SR; Ruby EG; Silver PA; Taha S; van den Engh G; Weiss PS; Wong GCL; Wright AT; Young TD Tools for the Microbiome: Nano and Beyond. ACS Nano 2016, 10, 6–37. [PubMed: 26695070]

67.) Braunschweig AB; Elnathan R; Willner I Monitoring the Activity of Tyrosinase on a Tyramine/Dopamine-Functionalized Surface by Force Microscopy. Nano Lett 2007, 7, 2030–2036. [PubMed: 17567175]

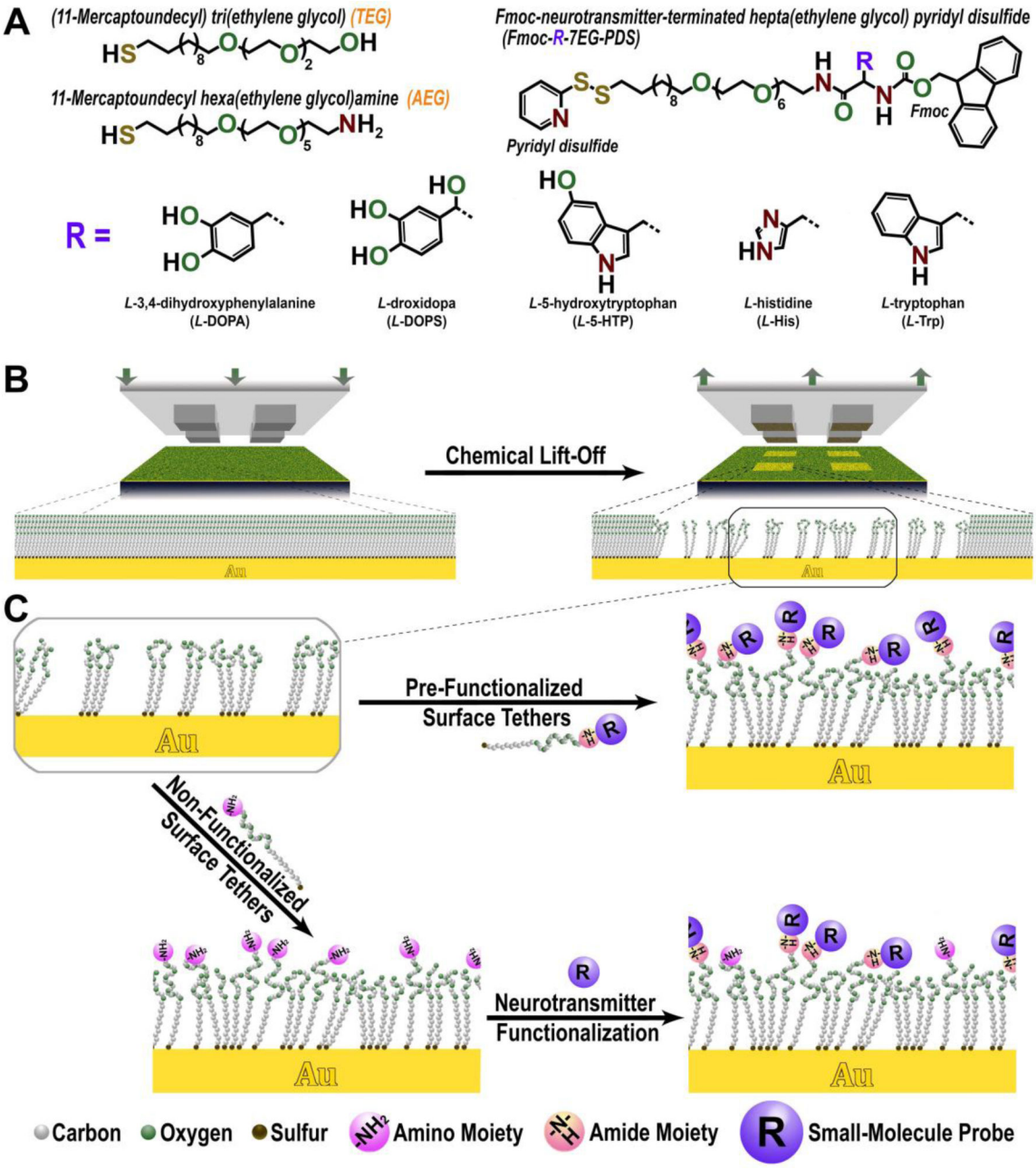

Figure 1.

(**A**) Structures of oligo(ethylene glycol)alkanethiols (TEG and AEG) and neurotransmitter pre-functionalized thiols (Fmoc-R-7EG-PDS). Pre-functionalized thiols consisted of pyridyl disulfide (PDS) head groups for self-assembly on Au surfaces, hepta(ethylene glycol)undecyl backbones (7EG) to resist nonspecific binding of biomolecule targets, neurotransmitter precursors (R) tail groups for biomolecule capture, and 9-fluorenylmethyloxycarbonyl groups (Fmoc) to protect neurotransmitter amino moieties during synthesis and self-assembly. The carboxyl groups of the neurotransmitter precursors were linked to 7EG backbones *via* amide bonds. (**B**) Polydimethylsiloxane stamps were treated with oxygen plasma to generate siloxyl groups for reaction with hydroxyl

tri(ethylene glycol)-terminated alkanethiol (TEG) self-assembled monolayers (SAM) on Au surfaces. During stamp/SAM contact, stamps removed ~70% of TEG molecules and associated underlying Au atoms in the contacted areas.[9,17] (**C**) Schematics (not to scale) of general patterning and functionalization strategies. Pre-functionalized thiols or thiol-tethers amenable to neurotransmitter post-functionalization were inserted into post-lift-off SAM regions.

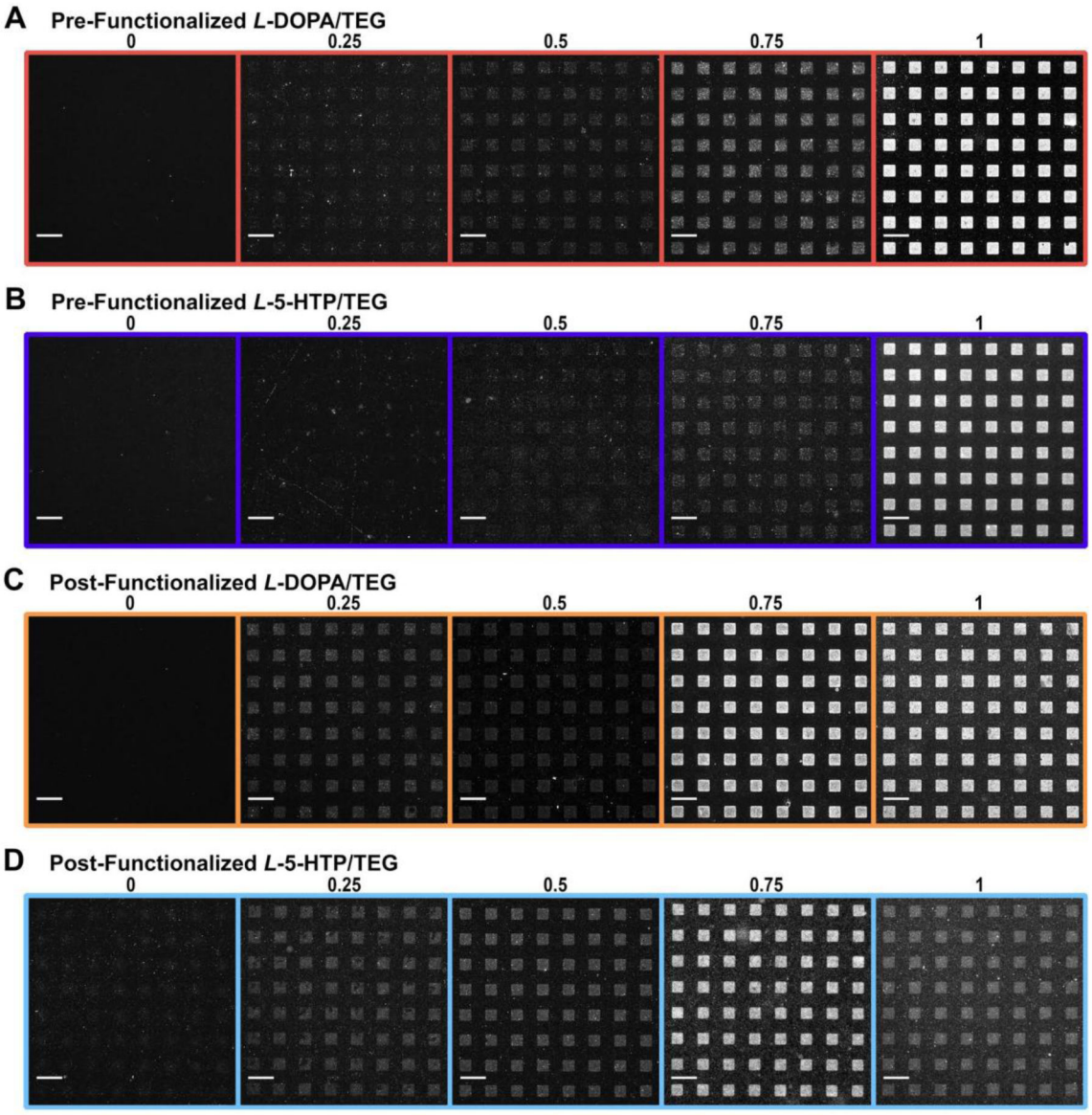

Figure 2.

Representative fluorescence images showing lift-off-lithography patterned self-assembled monolayers (SAMs) consisting of inserted pre-functionalized (**A**) *L*-3,4-dihydroxyphenylalanine (*L*-DOPA) thiols or (**B**) *L*-5-hydroxytryptophan (*L*-5-HTP) thiols, or inserted tethers post-functionalized with (**C**) *L*-DOPA (**D**) or *L*-5-HTP. Solution mole fractions of pre-functionalized thiols or amine-terminated hexa(ethylene glycol)alkanethiol (AEG) tethers *vs.* hydroxyl-terminated tri(ethylene glycol)alkanethiol (TEG) are shown above each image. Substrates were imaged at an emission wavelength of 525 nm (AlexaFluor® 488 with excitation at 490 nm) to visualize secondary antibodies, which recognize primary antibodies captured on patterned substrates. Scale bars are 50 μm.

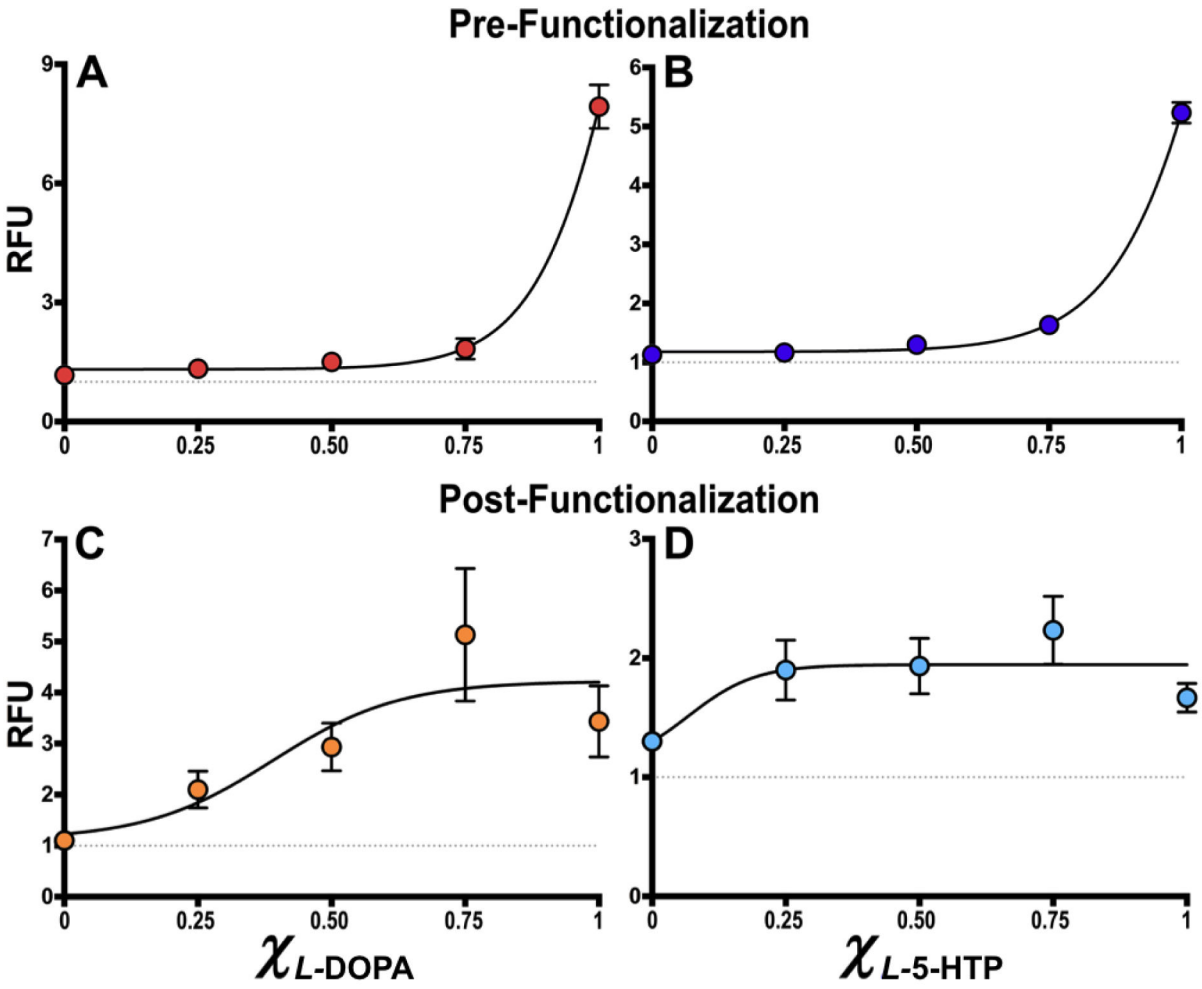

Figure 3.

Relative fluorescence intensities (RFU) *vs.* solution mole fractions (χ) of (**A,B**) pre-functionalized or (**C,D**) post-functionalized thiols relative to hydroxyl-terminated tri(ethylene glycol)alkanethiol (TEG). Data for *L*-3,4-dihydroxyphenylalanine (*L*-DOPA) are shown in (**A,C**); data for *L*-5-hydroxytryptophan (*L*-5-HTP) are in (**B,D**). Relative fluorescence intensities rose marginally with increasing fractions of pre-functionalized thiols suggesting preferential adsorption of TEG except where post-lift-off substrates were exposed to 100% pre-functionalized thiols, which resulted in maximal fluorescence intensities. Relatively small standard errors for the data in (**A,B**) suggest reproducible insertion and antibody recognition of pre-functionalized thiols. By contrast, relative fluorescence intensities for post-functionalized thiols rose at lower fractions of tether molecules during insertion in (**C**) for *L*-DOPA and (**D**) for *L*-5-HTP, where maximal fluorescence intensities were observed at <100% amine-terminated hexa(ethylene glycol)alkanethiol (AEG)/TEG mole fractions. Error bars for replicate samples were comparatively larger than for the post-functionalized approach suggesting greater variability across substrates. Error bars are standard errors of the means with N=3 samples per datum and are too small to be visualized in some cases.

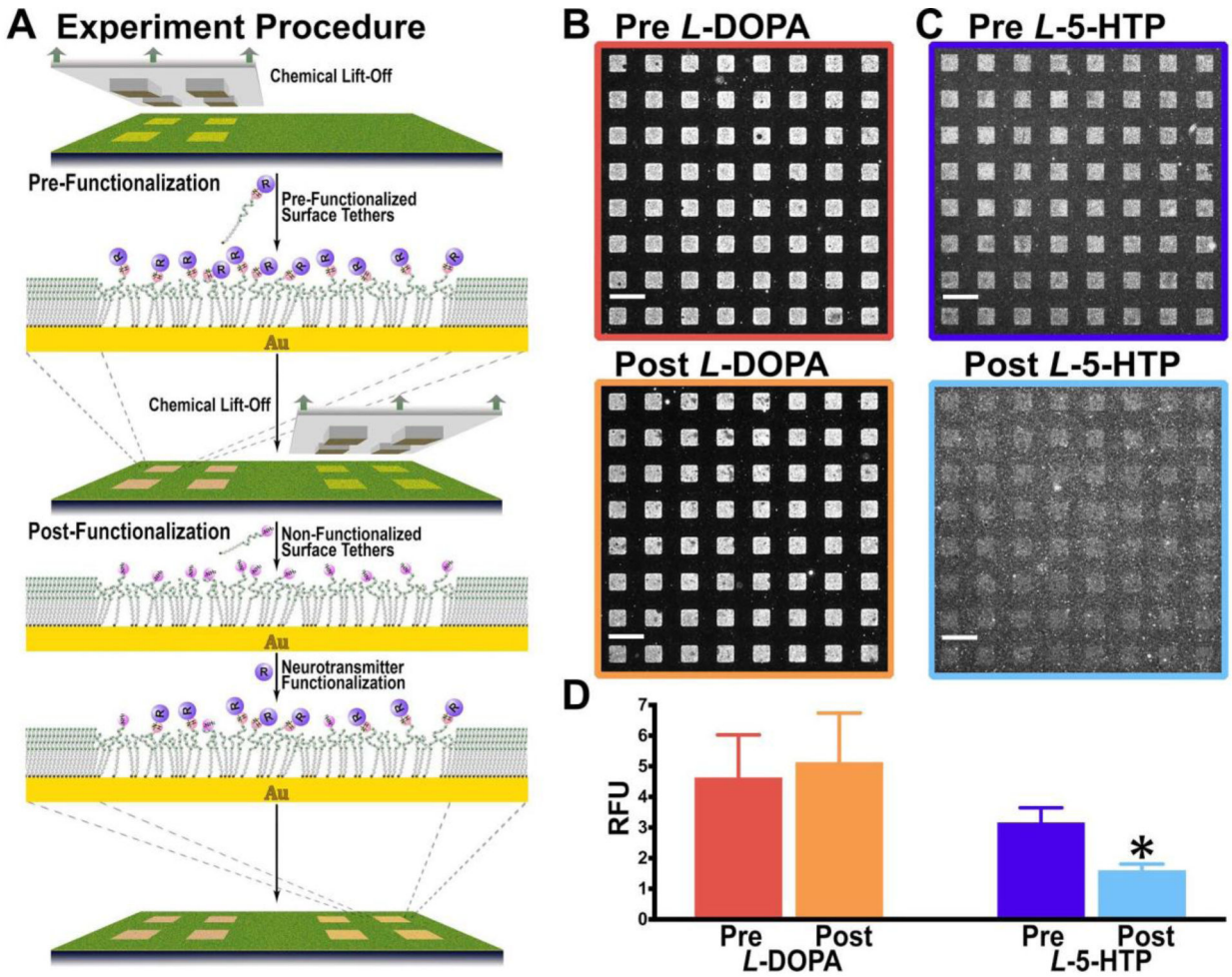

Figure 4.

(**A**) Schematic illustrating double lift-off lithography patterning with pre- followed by post-functionalized thiols. Pre-functionalized thiols were inserted after the first lift-off step. A second lift-off step was performed in an adjacent substrate region, tether molecules were inserted, and post-functionalization was carried out. (**B**) Representative fluorescence images for pre-functionalized *L*-3,4-dihydroxy-phenylalanine (*L*-DOPA) followed by post-functionalized *L*-DOPA. (**C**) Representative images of pre-functionalized *L*-5-hydroxytryptophan (*L*-5-HTP) followed by post-functionalized *L*-5-HTP. (**D**) Relative fluorescence intensities for antibody binding on double patterns of *L*-DOPA and *L*-5-HTP. Relative fluorescence intensities for pre-functionalized *vs.* post-functionalized *L*-DOPA were not significantly different. In contrast, higher relative fluorescence intensities were observed for pre-functionalized *vs.* post-functionalized *L*-5-HTP. Substrates were imaged at an emission wavelength of 525 nm (AlexaFluor® 488 with excitation at 490 nm). Error bars are standard errors of the means with $N=3$ substrates per group. For *L*-5-HTP $t(4)=3$ $^{*}P<0.05$. Scale bars are 50 μm.

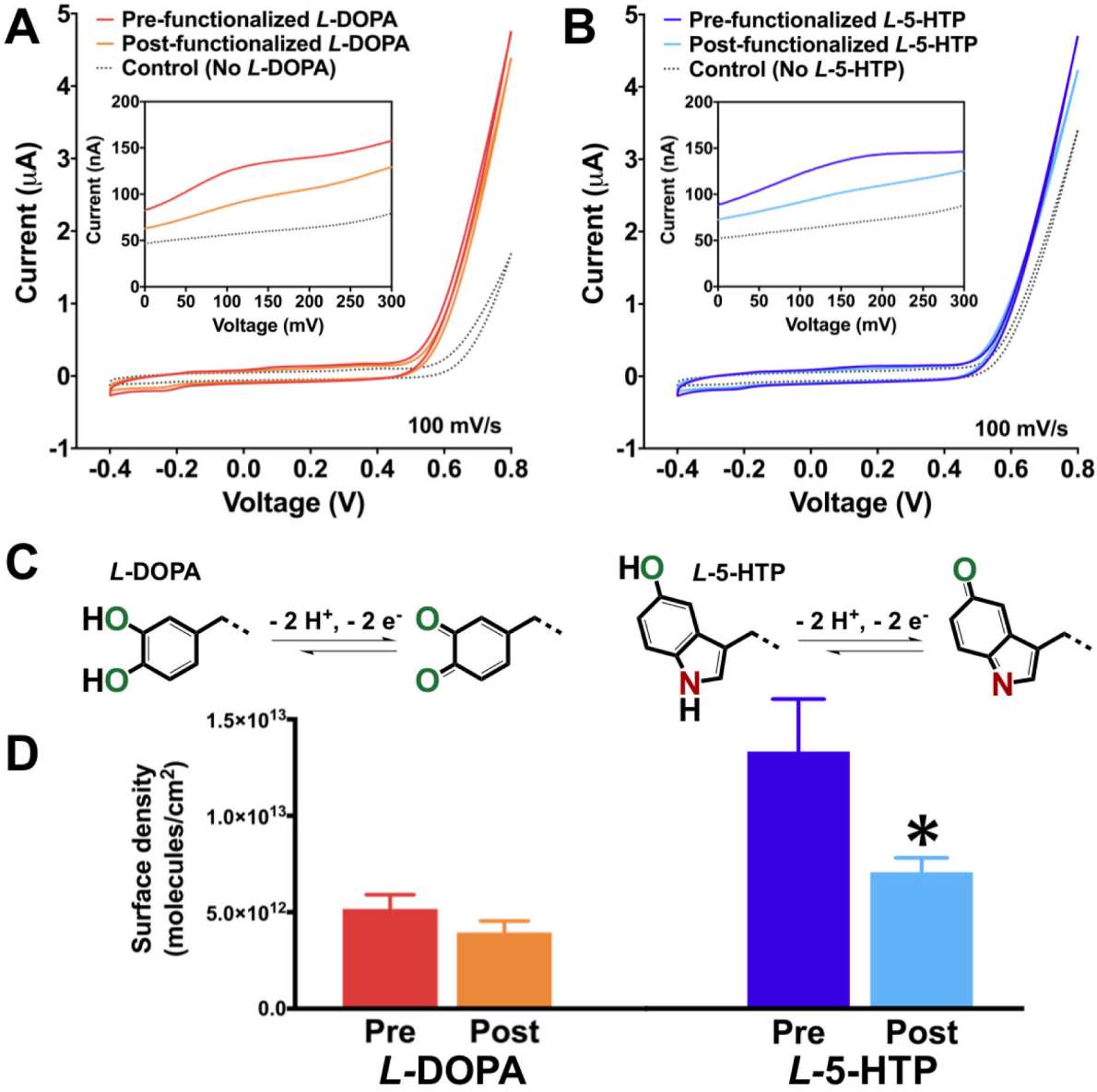

Figure 5.

Representative cyclic voltammograms (CVs) with insets showing the anodic peaks attributed to the oxidation of (**A**) *L*-DOPA or (**B**) *L*-5-HTP tethered to polycrystalline gold electrodes *via* pre-functionalized alkanethiols or post-functionalization of amine-terminated alkanethiols inserted within self-assembled monolayers of hydroxyl tri(ethylene glycol) undecanethiol (TEG) following lift-off lithography with featureless stamps. Representative CVs of control surfaces with unmodified amine-terminated alkanethiols inserted within SAMs of TEG following lift-off are shown in dotted black curves. The CVs in (**A,B**) were collected at a scan rate of 100 mV/s. (**C**) Two-electron oxidation/reduction of (**left**) *L*-DOPA and (**right**) *L*-5-HTP. (**D**) Surface densities of (**left**) *L*-DOPA pre- *vs.* post-functionalized thiol-modified substrates and (**right**) *L*-5HTP pre- *vs.* post-functionalized substrates. Error

bars are standard errors of the means with N=7–8 substrates per group; $t(13)=2$ *$P<0.05$ *vs.* pre-functionalized *L*-5HTP.

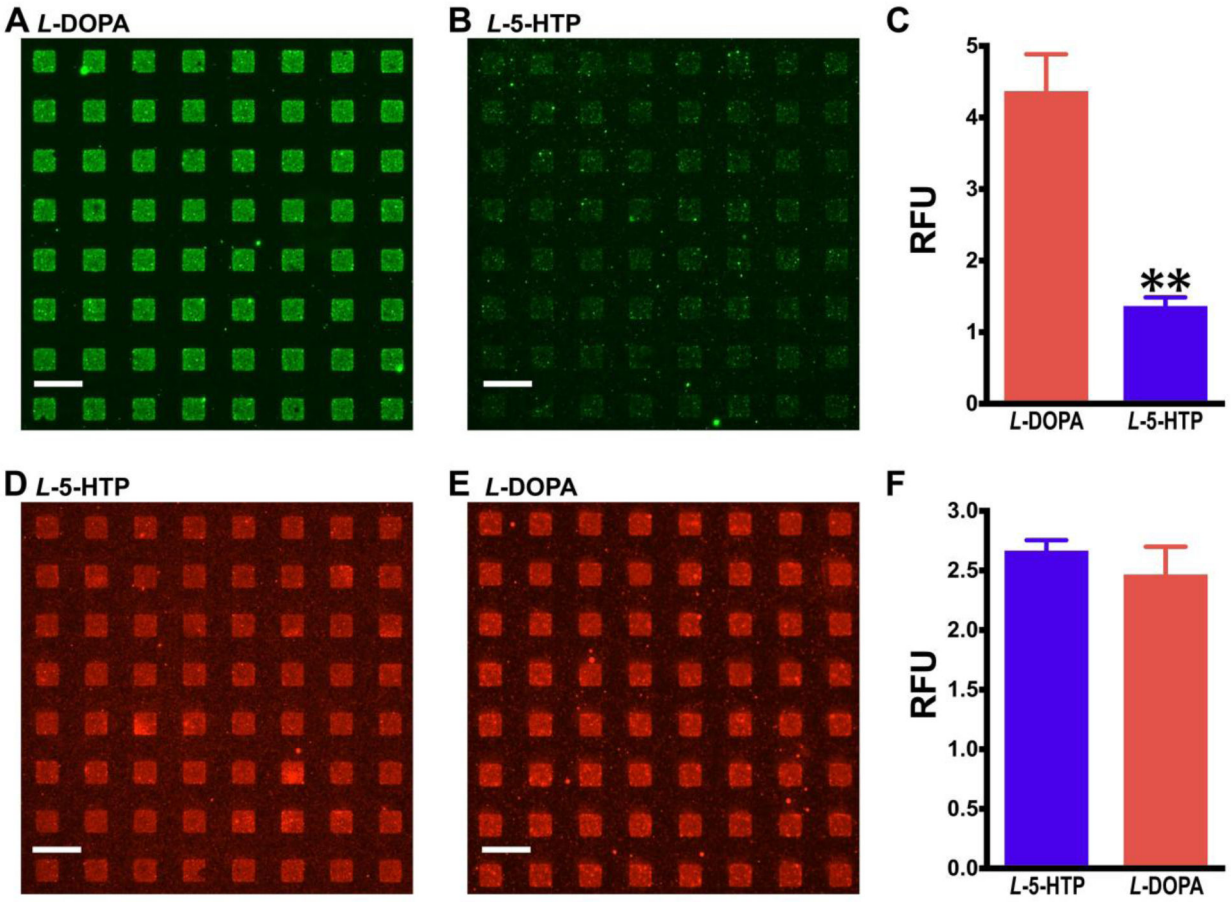

Figure 6.

Representative fluorescence images and relative fluorescence intensities for antibody binding on double lift-off lithography patterns of *L*-3,4-dihydroxyphenylalanine (*L*-DOPA) and *L*-5-hydroxytryptophan (*L*-5-HTP) pre-functionalized thiols. Substrates were imaged at two different emission wavelengths (525 nm (green, **A,B**) and 605 nm (red, **D,E**) for AlexaFluor 488 (excitation at 490 nm) and AlexaFluor 546 (excitation at 556 nm), respectively to visualize recognition of *L*-DOPA *vs.* *L*-5-HTP by anti-*L*-DOPA antibodies in (**A,B,C**). Recognition of *L*-5-HTP *vs.* *L*-DOPA by anti-*L*-5-HTP antibodies is seen in (**D,E,F**). Error bars represent standard errors of the means with $N=3$ substrates per group. Means are significantly different for anti-*L*-DOPA antibody binding $t(4)=6$ $^{**}P<0.01$. Scale bars are 50 μm.

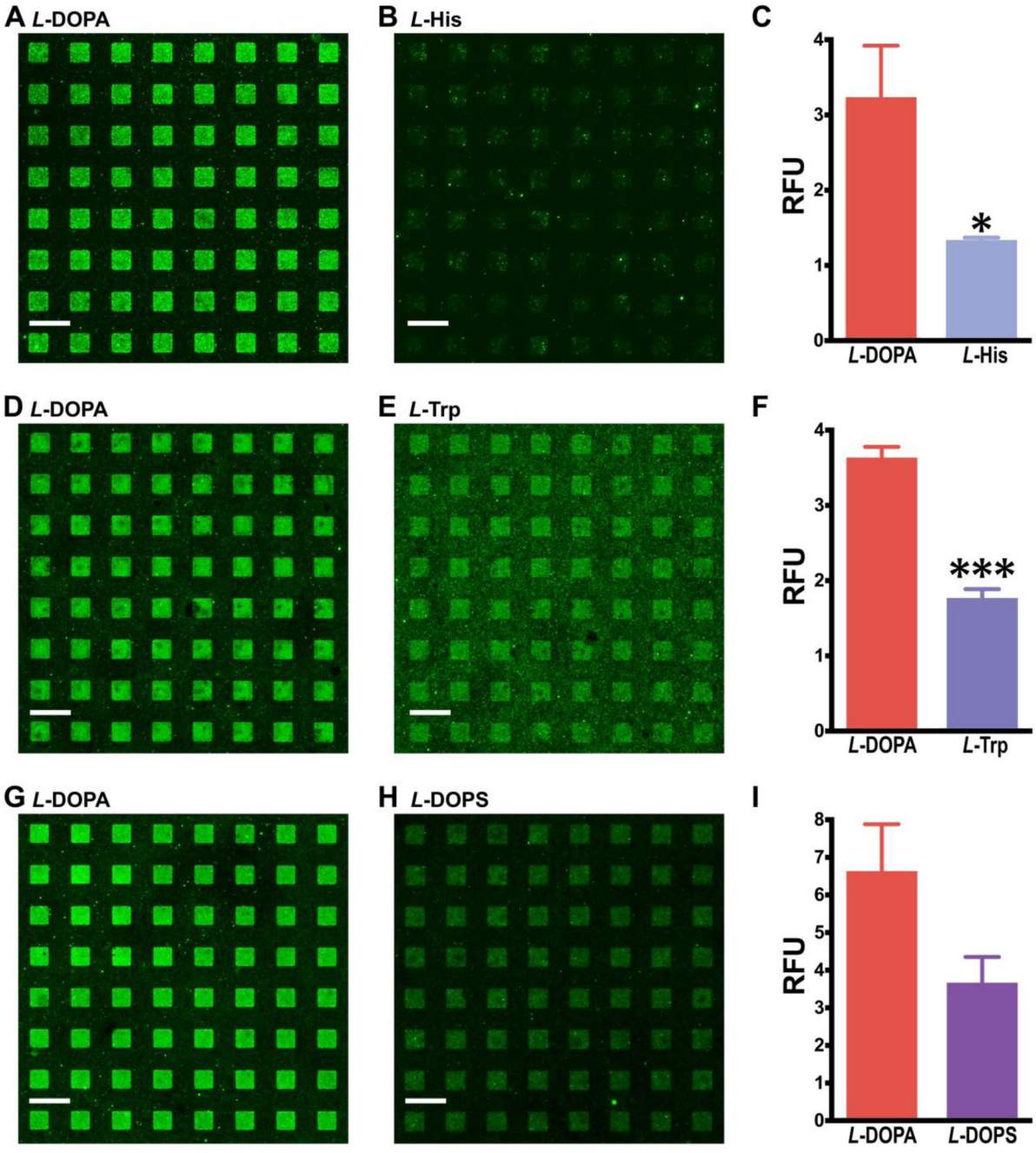

Figure 7.

Representative fluorescence images and intensity graphs for *L*-DOPA antibody binding on double lift-off lithography patterns of (**A,B**) *L*-3,4-dihydroxyphenylalanine (*L*-DOPA)/*L*-histidine (*L*-His), (**D,E**) *L*-DOPA/*L*-tryptophan (*L*-Trp), and (**G,H**) *L*-DOPA/*L*-droxidopa (*L*-DOPS) pre-functionalized thiols. Higher relative fluorescence intensities were observed for anti-*L*-DOPA antibody binding to surface tethered *L*-DOPA *vs.* (**C**) *L*-His and (**F**) *L*-Trp, but not (**I**) *L*-DOPS. Imaging was *via* AlexaFluor 488 labeled secondary antibodies (excitation at 490 nm and emission at 525 nm, green). Error bars are standard errors of the

means with N=3 substrates per group. Means are significantly different for (**C**) $t(4)=10$ *$P<0.05$ and **(F)** $t(4)=10$ ***$P<0.001$. **(I)** $t(4)=2$ $P>0.1$. Scale bars are 50 μm.

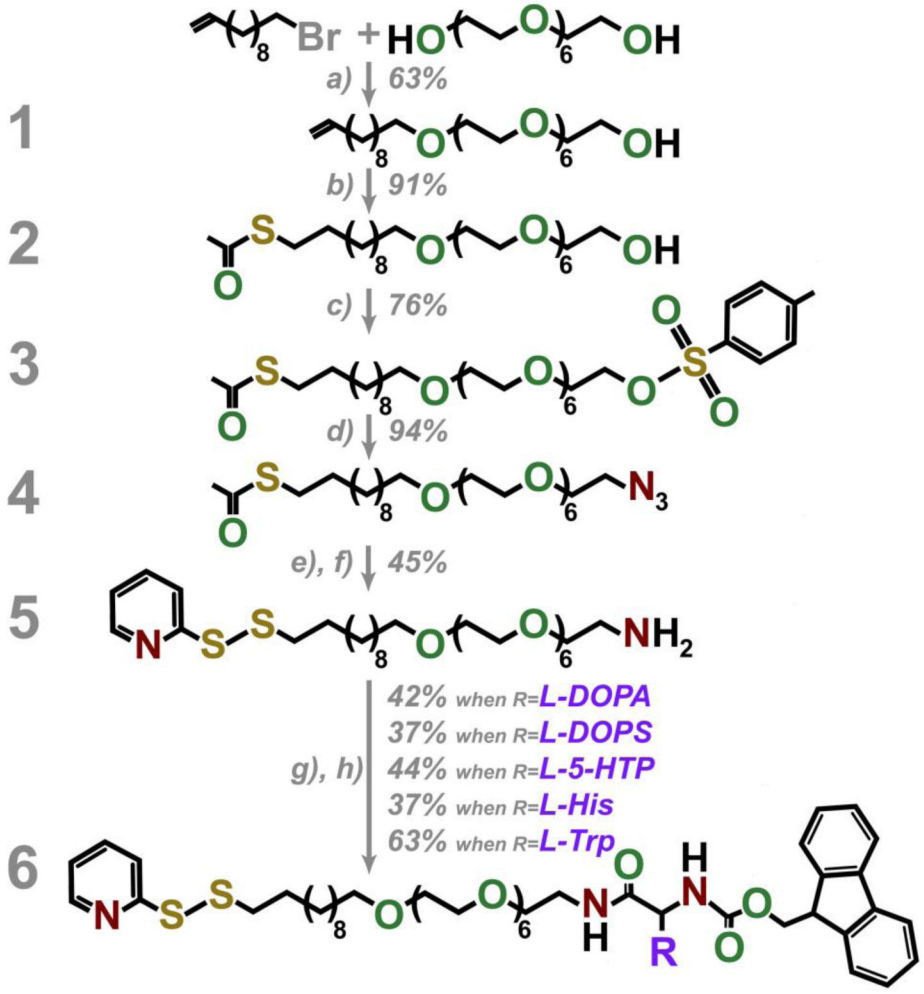

Scheme 1.

Synthesis of Fmoc-neurotransmitter-hepta(ethylene glycol)-pyridyl disulfide (Fmoc-R-7EG-PDS) compounds. a) 50% NaOH, 100 °C, 24 h; b) CH3COSH, AIBN, MeOH, UV, 48 h, room temperature; c) TsCl, TEA, DCM, 24 h, room temperature; d) NaN3, EtOH, 12 h, 85 °C; e) Ph3P, THF, 24 h, room temperature; f) 2-PDS, NH3 (7 N in MeOH), 72 h, room temperature; g) Fmoc-R, DIEA, HOBt, EDC, DCM (and/or DMF), 24 h, room temperature; and h) only for *L*-Trp and *L*-His, 20% TFA in DCM, 1 h, room temperature. Typical yields for each step are shown next to the arrows.